



TESI DE MÀSTER

Master

**MÀSTER UNIVERSITARI EN ENGINYERIA DE CAMINS,
CANALS I PORTS**

Títol

**SHEAR STRENGTH OF REINFORCED CONCRETE BEAMS
WITH FRP LONGITUDINAL AND TRANSVERSAL
REINFORCEMENT**

Autor

SANDRA ANDREEA GRADINARU

Tutors

**EVA OLLER IBARS
DENISE CARINA SANTOS FERREIRA**

Departament

ENGINYERIA DE LA CONSTRUCCIÓ

Intensificació

ESTRUCTURES

Data

Julio 2015

ABSTRACT

During the last decades the use of fiber reinforced polymers (FRP) has been introduced in the field of structural engineering, first as external reinforcement and later as passive and active reinforcement. The emergent interest in this material is due to its many advantages compared with the steel: it is more resistant and durable against corrosion, as well as, lighter and magnetically inert. These qualities allow decreasing the complexity, cost and cost of the reinforcement construction tasks while allowing the service life of structures to increase.

Nowadays, general shear resistance mechanisms in reinforced concrete are still under discussion. Specifically the use of FRP as shear reinforcement for concrete structures has not yet been deeply studied and the currently available data are insufficient to formulate rational design guidelines.

The effects of shear on the response of concrete beams with longitudinal and transversal FRP reinforcement is numerically studied in this work through a 1D non-linear fiber model accounting for the axial–bending–shear interaction. Experimental data from FRP RC beams available in literature, are compared with the numerical results. As this beam model is shear sensitive, the effects of shear in the structural response are evaluated. A good correlation in terms of ultimate loads, deflections, strains in the concrete and reinforcement is observed between the experimental data and the computed results. The numerical model is also able to reproduce the cracking widths and pattern when increasing the applied load.

Once the model is validated, it can be used to assess the accuracy of the analytical expressions present in the current codes of practice and contribute for their enhancement.

Keywords: *nonlinear numerical modeling, shear, FRP stirrups, reinforced concrete.*

Table of Contents

ABSTRACT	i
List of figures.....	v
List of tables	viii
1 Introduction	1
1.1 Problem statement	1
1.2 Objectives.....	2
1.3 Structure of the thesis.....	3
2 Beams reinforced with longitudinal and transversal FRP bars	4
2.1 FRP bars.....	4
2.1.1 Properties of the constituent materials	4
2.1.2 Properties of composite materials.....	10
2.2 Existing experimental programs of shear tests on concrete beams reinforced with longitudinal and transversal FRP.....	13
2.3 Analytical formulations for shear resistance of FRP reinforced concrete elements.....	19
2.3.1 (ACI-440.1R-06).....	22
2.3.2 (CNR-DT 204/2006).....	23
2.3.3 (JSCE 1997).....	24
2.3.4 (CSA S806-12).....	25
2.3.5 Proposal by (Fico et al. 2008).....	27
2.3.6 Proposal by (Nehdi et al. 2007).....	28
2.3.7 Proposal by (Hegger et al. 2009).....	28

3	Non-linear shear-sensitive fiber beam model	30
3.1.1	Structural scheme	30
3.1.2	Finite element	31
3.1.3	Sectional level	32
3.1.4	Material models	32
3.1.5	Representation of cracks	34
4	Numerical analysis of FRP RC beams	35
4.1	Description of the experimental campaign.....	35
4.1.1	General.....	35
4.1.2	Materials	36
4.1.3	Geometry	37
4.1.4	Experimental setup for shear tests.....	39
4.1.5	Failure modes.....	41
4.2	Numerical model.....	47
4.3	Comparison of numerical and experimental results.....	50
4.3.1	Test beam: S6BN-0.8-11	50
4.3.1.1	Load vs. displacement	52
4.3.1.2	Strains in the FRP longitudinal reinforcement	53
4.3.1.3	Strains in the FRP transversal reinforcement.....	54
4.3.1.4	Longitudinal strains in concrete	55
4.3.1.5	Transversal strain in the concrete web	56
4.3.1.6	Crack patterns.....	56
4.3.1.7	Other numerical results.....	59

4.3.2	Other tests beams.....	61
4.3.2.1	Load vs displacement	61
4.3.2.2	Strains in the FRP longitudinal reinforcement	62
4.3.2.3	Strains in the FRP transversal reinforcement.....	63
4.3.2.4	Longitudinal strains in concrete	65
4.3.2.5	Transversal strain in the concrete web	66
5	Conclusions	67
	References	70

List of figures

Figure 1: Basic material components that are combined to create an FRP composite (BaNthia et al. 2006)	4
Figure 2: Diagram stress-strain of FRP (BaNthia et al. 2006).....	5
Figure 3: Stress-strain properties of typical fibers.(BaNthia et al. 2006)	7
Figure 4: failure in stirrups at the bent zone of L05-1 (Bentz et al. 2010).....	16
Figure 5: Flexural compression failure in constant moment region of L20-2(Bentz et al. 2010). 16	
Figure 6: Types of shear failure in experimental trials(Spadea 2010)	17
Figure 7: Limiting strain according to the Strain Approach(<i>Clarke 1996</i>)	21
Figure 8: General characteristics of the fiber beam models (Ferreira 2013)	31
Figure 9: Fiber beam model in CONSHEAR: a) general characteristics b) finite element for the 2D case (Ferreira 2013).....	31
Figure 10: Assumptions of the model at the section level (Ferreira 2013)	32
Figure 11: Constitutive model for the concrete: (a) smeared crack, (b) compression, (c) tension (Ferreira 2013)	33
Figure 12: Constitutive model for the reinforcement (Ferreira 2013)	33
Figure 13: Scheme of the post-processing method for the representation of the cracks (Ferreira 2013)	34
Figure 14: Experimental tests on the beam (Kurth 2012)	35
Figure 15: Reinforcement drawing (Kurth 2012).....	38
Figure 16: Type of stirrups (Kurth 2012).....	38
Figure 17: Experimental set-up of shear tests (Kurth 2012)	39
Figure 18: Metrology of concrete (Kurth 2012).....	40

Figure 19: Metrology of reinforcement (Kurth 2012).....	41
Figure 20: Cracking at failure in experimental S4AH-0.8-7 ($\rho_w = 0.75\%$, $f_{cm} = 42.2 \text{ N/mm}^2$ (Kurth 2012)	41
Figure 21: Damaged stirrups (Type A and B) after failure in experiments with a shear reinforcement degrees ρ_w of 0.75% (Kurth 2012).....	42
Figure 22: Damaged double headed bolt (type C) after failure while trying S12CH-0.7-23 ($\rho_w = 0.75\%$, $f_{cm} = 73.1 \text{ N / mm}^2$)(Kurth 2012)	42
Figure 23: Cracking at failure in experimental S6BN-2.3-12 ($\rho_w = 2.26\%$, $f_{cm} = 30.7 \text{ N / mm}^2$)(Kurth 2012)	43
Figure 24: Cracking at failure in experimental S2AN-2.3-4 ($\rho_w = 2.26\%$, $f_{cm} = 33.5 \text{ N / mm}^2$)(Kurth 2012)	43
Figure 25: Discretization of the cross section.....	47
Figure 26: Shear resistant zone	47
Figure 27: Discretization of the beam.....	48
Figure 28: Longitudinal and transversal reinforcement of the test beams (Kurth 2012)	49
Figure 29: FRP stirrups configurations (Kurth 2012)	49
Figure 30: Plan of reinforcement for test beam: S6BN-0.8-11(Kurth 2012)	50
Figure 31: Beam cross-sections for test beam: S6BN-0.8-11(Kurth 2012).....	50
Figure 32: Metrology of concrete and sensors considered for comparison with the numerical results (Kurth 2012)	51
Figure 33: Metrology of reinforcement and sensors considered for comparison with the numerical results(Kurth 2012)	51
Figure 34: Experimental and numerical deflection in the center of the beam for test S6BN-0.8-11	52

Figure 35: Experimental and numerical results for the strains in longitudinal FRP reinforcement for test S6BN-0.8-11.....	53
Figure 36 : Experimental and numerical results of Strains in stirrups along the length of the beam for test S6BN-0.8-11	54
Figure 37: Experimental and numerical results of concrete deformation for test S6BN-0.8-11 .	55
Figure 38: Shear-strain of concrete numerical and experimental results for test S6BN-0.8-11 ..	56
Figure 39: Cracking width for test S6BN-0.8-11.....	58
Figure 40: Location of measured cracks	58
Figure 41: Strain in the stirrups for different positions of the sensors test S6BN-0.8-11	59
Figure 42: Strains in stirrup height at the bent zone for testS6BN-0.8-11	60
Figure 43: Experimental and numerical deflection in the center of the beam for tests S2AN-0.8-3, S4AH-0.8-7, S8BH-0.8-15 and S10CN-0.7-19	61
Figure 44: Experimental and numerical results of strains in the FRP longitudinal reinforcmenet for tests S2AN-0.8-3, S4AH-0.8-7, S8BH-0.8-15 and S10CN-0.7-19.....	62
Figure 46: Experimental and numerical results of strains in stirrups along the length of the beam for tests S2AN-0.8-3, S4AH-0.8-7, S8BH-0.8-15 and S10CN-0.7-19.....	64
Figure 45: Experimental and numerical results of longitudinal concrete deformation for tests S2AN-0.8-3, S4AH-0.8-7, S8BH-0.8-15 and S10CN-0.7-19	65
Figure 47: Numerical and experimental of transversal strain in the concrete web results for tests S2AN-0.8-3, S4AH-0.8-7, S8BH-0.8-15 and S10CN-0.7-19	66

List of tables

Table 1: Properties of the composite matrix (Alzate 2012).....	6
Table 2: Properties of the glass fibers (Feldman 1989, Kim 1995).....	8
Table 3: Properties of the carbon fibers (Feldman, 1989).....	9
Table 4: Properties of the aramid fibers (Feldman, 1989)	9
Table 5: Properties of fiber reinforced polymers	12
Table 6: Limit strain value(Fico et al. 2008).....	27
Table 7: Characteristics of longitudinal reinforcement (Kurth 2012).....	36
Table 8: Characteristics of transversal reinforcement (Kurth 2012)	37
Table 9: Types of failure for the experimental beams.....	44
Table 10: Beam dimensions, concrete properties, longitudinal reinforcement, and transversal reinforcement(Kurth 2012).....	46
Table 11: Cracking patterns at different load levels for test S6BN-0.8-11	57

1 Introduction

1.1 Problem statement

Fiber reinforced polymer (FRP) bars can be an advantageous alternative to steel bars for internal reinforcement of concrete structures, especially in environments exposed to corrosion. In these type of environments, the use of FRP stirrups, that are normally located as an outer reinforcement, has even more sense as it can be more susceptible to severe environmental effects, due to the minimum concrete cover provided.

The use of FRP as reinforcement for concrete structures has increased rapidly over the last years. FRP reinforcement is made from high-tensile-strength fibers, such as carbon, glass, aramid and others, embedded in polymeric matrices and produced in the form of bars, strands, ropes, tendons and grids, in a wide variety of shapes and characteristics. FRP reinforcement is used as prestressed, non-prestressed, longitudinal and transversal reinforcement for concrete structures.

While flexural mechanisms are clearly established, there is not a consensus among the engineers and scientists about how to predict, for design purposes, the shear strength of FRP reinforced concrete beams.

In relation to the mechanical properties of the FRP reinforcement, the main differences in comparison with steel, are the lower modulus of elasticity and a linear elastic behaviour up to failure which implies a lack of plasticity and a brittle behaviour in failure. It also presents a reduced elasticity modulus that can compromise its use in terms of deflection limitations in service limit states.

Precisely due to this difference in the mechanical properties of both materials, the failure modes that commonly occur in reinforced FRP elements are different from those with conventional steel. This indicates the need for a new design methodology that is specific for the study of FRP reinforced concrete elements, able to reproduce the various sources that contribute to the shear resistance mechanism. Numerical models able to reproduce the

nonlinear response of such elements, from elastic to cracked and ultimate phases, allow to study in detail the structural response. In fact, numerical models, after being verified and validated with experimental benchmarks, can contribute to enhancing the models present in the codes of practice.

Regarding large-scale structural analysis, the use of complex 2D or 3D finite element (FE) programs can be impracticable due to the inherent computational costs, the difficulty to evaluate the many input variables required by the model and the demanding task of analyzing the vast amount of output data. Instead, fiber beam models represent may attain a good compromise between simplicity and accuracy allowing for complex nonlinear analysis without the need of a great computational cost and permitting a more straightforward results interpretation.

1.2 Objectives

The main objective of the thesis is to improve the knowledge related to the behaviour and performance of beams reinforced with longitudinal and transversal FRP.

For this purpose, an experimental campaign was numerically simulated with a FE model. . To perform these, an extended review of the state of the art was firstly performed in order to choose an existing experimental program that is well-documented and presents relevant results.

The numerical analysis were carried out with a non-linear shear sensitive fiber beam model implemented into the computer program CONSHEAR (Ferreira et al. 2013).

The numerical model was validated by comparing the computed results with the experimental data available in the literature. This study aimed to check the validity of the model to analyze FRP reinforced concrete specimens.

After validating the model, it is used to study more deeply the structural response by analyzing variables related with shear, such as, distortions, flow of strains in the stirrups. This aims to be a

contribution to the understanding of the shear mechanism in FRP reinforced concrete elements.

Another goal of the work is to compare the experimentally ultimate strain in the bent zone with the predicted results from the numerical approach and also with the proposed limit strain in the guidelines.

It is also aimed that, after being validated, the model is ready to be used in analysis of real scale structures, as a continuation of the present work.

1.3 Structure of the thesis

The thesis is divided in 5 chapters.

Chapter 1 is the present introduction where the current problems regarding the use of longitudinal and transversal FRP reinforcement and the objectives of the thesis are presented and contextualized.

Chapter 2 describes the main characteristics of FRP as a composite material, the different existing experimental programs detailing the failure modes of the tested specimens, and the main existing theoretical models that predict the shear strength of reinforced concrete elements with transversal FRP reinforcement.

Chapter 3 resumes the theoretical background of the computer program used in this thesis (CONSHEAR).

Chapter 4 describes the experimental campaign studied in this work - specimens tested by (Kurth 2012). It also presents the numerical model, and a comparison between the available experimental data and the numerical results. Finally, further numerical results related with shear response are presented and discussed.

Chapter 5 points out the main conclusions obtained from this work and describe several proposals for future lines of research to complement and continue this thesis.

2 Beams reinforced with longitudinal and transversal FRP bars

2.1 FRP bars

2.1.1 Properties of the constituent materials

The mechanical properties of FRP bars are different from those of steel bars and depend mainly on both on the type of matrix and fibers, as well as, on their volume fraction. Generally FRP bars present lower weight, lower Young's modulus and higher ultimate strength than steel. The most commonly used fiber types in structural engineering are the carbon (CFRP), the glass (GFRP) and the aramid (AFRP) fibers.

The combination of both materials, fibers and matrix, results in a composite with enhanced properties (Figure 1). The fibers provide rigidity and strength while the matrix ensures bound to the compound and allows the correct distribution of stresses between the fibers and the bonding surface, also preventing corrosion.

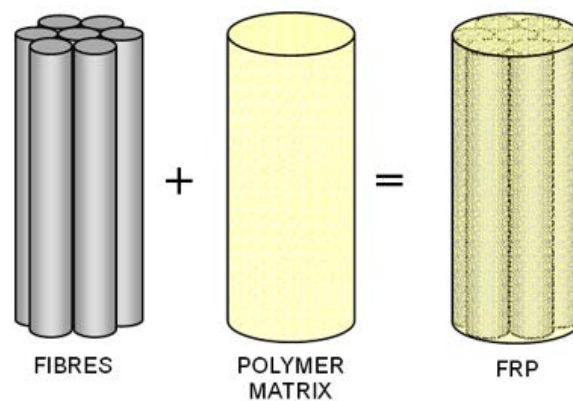


Figure 1: Basic material components that are combined to create an FRP composite (BaNthia et al. 2006)

The mechanical properties of the compound are obtained by the rule of mixtures and depend on the quality of the fibers and their orientation, as well as, the adhesion to the matrix and the

volumetric amount of materials. In the direction perpendicular to the fibers laminate, the mechanical properties may be lower than those of its components.

In Figure 2 can be observed the high strain capacity of the matrix comparing with the fibers.

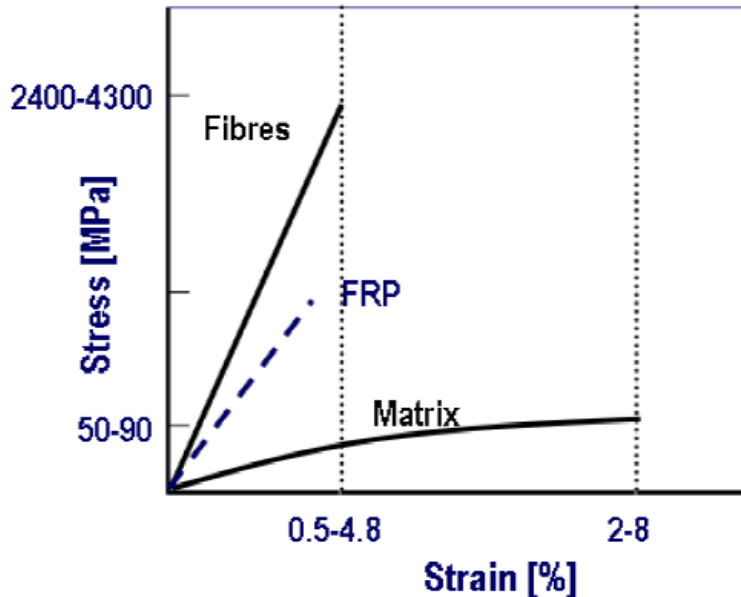


Figure 2: Diagram stress-strain of FRP (BaNthia et al. 2006)

Matrix

The main functions of the matrix within the compound are maintaining cohesion between the fibers, ensuring uniform distribution of stresses, providing the geometric configuration of the material and protect it from external agents that can damage or compromise its mechanical properties. Furthermore, it presents a good behaviour in compression and shear, thus improving the properties of the composite.

The choice of matrix material will determine the properties of the new material, which must be considered, in each case, the best option according to the objectives to pursue.

Matrix materials for FRPs can be grouped into two broad categories: thermoplastics and thermosetting resins.

Thermoplastics include such polymer compounds as polyethylene, nylon and polyamides.

Thermosetting are the most common in civil engineering because they have less loss of rigidity at high temperatures. Typically are polyesters, vinyl esters or epoxy resins, which are the most used due to enhanced strength and rigidity; but are more expensive.

Generally, these resins have a linear-elastic response until failure, but with a much lower modulus of elasticity than fibers.

Due to the non-structural importance of the resins, as well as their high cost, a minimum resin volume ratio is always desirable. However, the maximum fiber ratio that can be achieved is normally below 70%.

Table 1 indicates the common values for the mechanical properties of the different type of materials that can be used as composite matrix of the FRP.

Material	Modulus of elasticity (GPa)	Tensile Strength (MPa)	Ultimate strain (%)	Density (kg/m³)
Polyester	2.1-4.1	20-100	1.0-6.5	1000-1450
Vinylester	3.2	80-90	4.0-5.0	-
Epoxy	2.5-4.1	55-130	1.5-9.1	1100-1300

Table 1: Properties of the composite matrix (Alzate 2012)

Fibers

The fibers provide the strength and stiffness of an FRP. Due to the fact that fibers used in most structural FRP applications are continuous and are oriented in specified directions, FRPs present orthotropic mechanical behaviour, and they are much stronger and stiffer in the fiber direction(s).

Fibers are generally selected to have high stiffness, high ultimate strength, low variation of strength between individual fibers, stability during handling and uniform diameter.

Many different types of fibers are available, presenting specific advantages and disadvantages. In civil engineering applications, the three most commonly used fiber types are glass, carbon (graphite), and to a lesser extent, aramid. The suitability of the various

fibers for specific applications depends on a number of factors including the required strength, the stiffness, durability considerations, cost constraints, and the availability of component materials.

Figure 3 shows typical stress-strain curves for various types of fibers. Note that these curves are for the pure fibers only, and they do not include the effects of the polymer matrix.

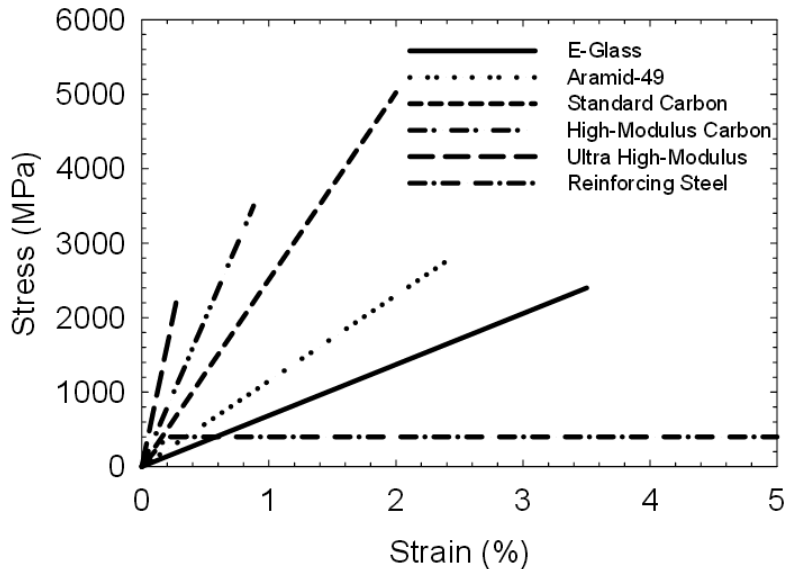


Figure 3: Stress-strain properties of typical fibers. (BaNthia et al. 2006)

It can be observed that FRP materials, unlike steel, do not offer plasticity, and have a linear-elastic behaviour till rupture; also present a higher ultimate strength than conventional steel.

As can be observed in Figure 3, the modulus of elasticity of the glass and aramid fibers is lower than that of steel; the standard carbon and high-modulus carbon fibers present very similar elasticity modulus, and ultra-high modulus carbon is clearly superior. It can also be seen that, while the ultimate strength of aramid, glass and ultra-high modulus carbon fibers are very similar, the standard carbon fibers strength is far superior.

Contrasting with the ductile response exhibited by steel, FRP fibers do not yield before failure, presenting small deformations near failure; this is the reason why most codes and analytical models limit the deformation of FRP to avoid brittle failures.

Typical FRP reinforcement products are grids, bars, fabrics, and ropes. The bars have various types of cross-sectional shapes (square, round, solid, and hollow) and deformation systems (exterior wound fibers, sand coatings, and separately formed deformations).

Subsequently, the 3 types of fiber studied are presented in more detail.

- *Glass fibers*

Glass fibers are the most economical, and consequently the most commonly used fibers in structural engineering applications. They are characterized by their high strength, low thermal conductivity and low stiffness that can lead to excessive deformations in structures reinforced with this type of material.

There are several different grades available, but the most common are E-glass and the more expensive, but stronger, R-glass.

Table 2 shows the typical range of values of the mechanical properties of these types of fiber.

Type	Modulus of elasticity (GPa)	Tensile Strength (GPa)	Ultimate strain (%)
E	70	1.9 – 3.0	3.0 – 4.5
S	85-90	3.5 – 4.8	4.5 – 5.5

Table 2: Properties of the glass fibers (Feldman 1989, Kim 1995)

- *Carbon fibers*

The carbon fibers have a very high ultimate strength, and are used to replace glass in those cases where the stiffness of the latter are insufficient, since the elastic modulus of the carbon fibers is considerably greater. This material has a high price due to the difficulty and cost of its production process.

It presents a good resistance to thermal, chemical, and environmental effects, also good fatigue behaviour.

Carbon fibers are an ideal choice for structures which are weight and/or deflection sensitive.

There are 2 types of carbon fiber: the high resistance (RH) and high modulus (HM) whose characteristics are shown in Table 3.

Type	Modulus of elasticity (GPa)	Tensile Strength (GPa)	Ultimate strain (%)
HR	215 – 235	3.5 – 4.8	1.4 – 2.0
HM	350 – 500	2.5 – 3.1	0.5 – 0.9

Table 3: Properties of the carbon fibers (Feldman, 1989)

- *Aramid*

Aramid fibers are characterized by high strength and good fatigue behaviour. They have a high modulus of elasticity, showing little deformation at failure. However, despite having a high tensile resistance, the compressive behaviour is not linear and ductile.

They have an anisotropic structure, which have better performance in the direction of the fiber and are industrially available in both continuous and discontinuous form. This material presents resistance to chemical attacks, but has low resistance to ultraviolet radiation. Its common mechanical characteristics are indicated in Table 4.

Type	Modulus of elasticity (GPa)	Tensile Strength (GPa)	Ultimate strain (%)
High module	115 – 130	3.5 – 4.0	2.5 – 3.5
Low module	70 – 80	3.5 – 4.1	4.3 – 5.0

Table 4: Properties of the aramid fibers (Feldman, 1989)

2.1.2 Properties of composite materials

The properties of the resulting composite material will be conditioned by the type of matrix and the type of fiber chosen and by the volumetric amount and orientation.

Thereof the modulus of elasticity of the composite material can be obtained by applying the so-called "rule of mixtures", which allows to express the properties of a compound according to the properties of materials that comprise it (in this case the matrix and fibers) and their volume fractions. This requires making the assumption that the bond between the fiber and the matrix is perfect, so there is no discontinuity in the deformation ϵ through the interface when a tensile or compressive load is applied in the direction parallel of the fibers. Hence, compatibility of deformations is assumed:

$$\epsilon_c = \epsilon_f = \epsilon_m \quad (2.1)$$

If the materials are considered perfectly elastic, the stresses σ can be calculated as:

$$\sigma_m = E_m \epsilon_m \quad (2.2)$$

$$\sigma_f = E_f \epsilon_f \quad (2.3)$$

The load supported by the composite F_c can be expressed as the sum of the loads carried by the matrix F_m and the fibers F_f , according to the following expression:

$$F_c = F_m + F_f \quad (2.4)$$

In terms of stress σ :

$$\sigma_c A_c = \sigma_m A_m + \sigma_f A_f \quad (2.5)$$

With A_c , A_m , A_f representing respectively the sectional areas of the composite, the matrix, and fiber.

Dividing equation (2.5) by A_c results in:

$$\sigma_c = \sigma_m \frac{A_m}{A_c} + \sigma_f \frac{A_f}{A_c} \quad (2.6)$$

Where the following expression of volume fractions V can be set as:

$$V_m = \frac{A_m}{A_c} \quad (2.7)$$

$$\sigma_f = E_f \varepsilon_f \quad (2.8)$$

Rewriting equation (2.6) comes:

$$E_c = E_m \cdot V_m + E_f \cdot V_f \quad (2.9)$$

Where E_c is the elastic modulus of the composite, E_m the elastic modulus of the matrix, and E_f the elastic modulus of the fiber.

And, since the volume of the matrix V_m plus the volume of the fibers V_f is equal to 1:

$$V_m + V_f = 1 \quad (2.10)$$

Equation (9) can be rewritten as:

$$E_c = E_m \cdot (1 - V_f) + E_f \cdot V_f \quad (2.11)$$

Consequently the elastic modulus of FRP composite material can be obtained as the sum of the modulus of elasticity multiplied by their volume fractions components.

FRP products are characterized by having an elastic behaviour to failure, and to develop a high tensile strength (greater than steel) in the direction of the fibers. This anisotropy considerably affect the shear strength, which is very small compared to the tensile strength.

In summary, the main advantages of FRP as structural reinforcement material are:

- High resistance to corrosion;
- Lightweight;
- High tensile resistance;
- reduced installation time and cost;
- Low maintenance;
- Good behaviour to fatigue.

There are also some disadvantages that must be taken into account in the design in order to avoid inadequate structural response, such as:

- Brittle failure because there is no plastic branch and therefore no ductility;
- Lower modulus of elasticity or similar to steel, that may lead to high deformations;
- High cost;
- High vulnerability of the matrix at elevated temperatures.

The reduced weight of the fibers compared to steel and concrete and their high resistance / weight ratio is one of the characteristics that make them more attractive to structural applications. This allows not only significant savings in material (which is very significant because of its high cost) but also facilitates the construction process.

Table 5 summarizes the main characteristics of composite materials FRP.

Unidirectional composite materials	Fiber weight (%)	Density (kg/m³)	Tensile elastic module (GPa)	Tensile Strength (GPa)
Glass-Polyester(GFRP)	50-80	1600-2000	20-55	400-1800
Carbon-Epoxy (CFRP)	65-75	1600-1900	120-250	1200-2250
Aramid-Epoxy(AFRP)	60-70	1050-1250	40-125	1000-1800

Table 5: Properties of fiber reinforced polymers

2.2 Existing experimental programs of shear tests on concrete beams reinforced with longitudinal and transversal FRP

The use of FRP as reinforcing material in structural concrete is relatively new. Several research groups worldwide are recently dedicated to the experimental and numerical study of the structural behaviour of concrete elements reinforced with FRP. As bending behaviour in RC is seen as solved by the actual state-of-the-art, the main concern now is shear. This is the reason why this work is focused on shear tests.

In conventionally steel RC beams, there are different failure modes depending on the longitudinal and transversal reinforcement ratios and on the shear span to depth ratio. FRP RC beams with FRP stirrups present different failure modes due to the linear elastic behaviour of the FRP reinforcement.

In steel RC beams, if the longitudinal reinforcement ratio is low, failure may be often due to a flexural-shear mechanism. Usually, first flexural cracks initiate, and subsequently develop inclined through the web. As the load increases, damage concentrates around the so-called shear critical crack. After increasing the applied load, a second branch of the crack develops inside the concrete chord, eventually connecting the first crack and the point where the load is applied, producing failure. For this type of failure, the increment of tensile force in the longitudinal reinforcement due to the inclined crack, which depends on the shear force, will commonly produce yielding of the longitudinal reinforcement.

This is not the case for FRP longitudinal reinforcement, which is linear elastic up to failure, and which has an ultimate tensile strength higher than the steel yielding stress. In addition, designers are often required to use FRP longitudinal reinforcement ratios higher than the balanced reinforcement ratios to meet the serviceability criteria.

If the longitudinal reinforcement ratio is high enough, the transversal steel stirrups of steel RC beams might yield, and concrete chord crushing can be observed (brittle shear failure). This

type of failure can also develop in FRP RC beams with FRP stirrups. However, in this case, concrete crushing will occur if the FRP stirrups do not have previously failed locally in the bent zone.

Finally, in thin-walled beams, the web of the beam can crush if the inclined compressive stresses exceed the concrete strength.

The failure modes of some of the existing experimental programs have been analysed to evaluate the shear behaviour of FRP RC beams with FRP stirrups. As experimentally observed, the main difference of the shear behaviour of beams with FRP stirrups compared to conventional beams with steel stirrups is that stirrups do not yield, and they usually fail in their bottom bent zone. This type of failure can be explained by the fact that bending of the FRP bars into the stirrups configuration, significantly reduces its strength at the bent portions, due to their unidirectional characteristics.

A summary of the response and failure modes of some of the existing experimental programs is presented in the following.

- (Nagasaka et al. 1933)

(Nagasaka et al. 1933), tested 35 half-scale rectangular beams with different type (CFRP, GFRP, AFRP, Hybrid, steel) and ratio (0, 0.5, 1.0 and 1.5%) of transversal reinforcement, different concrete strengths and clear span. Half of the specimens with FRP stirrups (12 out of 24 tests) failed due to breaking of the stirrups at the bent zone and the rest of the specimens failed due to the crushing of concrete struts formed between two adjacent diagonal cracks or by crushing from flexural-compression.

- (Ahmed et al. 2010)

The experimental campaign by Ahmed et al. (2010) consisted on 3 beams with T-shape section with CFRP stirrups of 9.5mm diameter with different spacings. The tensile strength of the stirrups was around $f_{tu} = 1538 \text{ N/mm}^2$ and their bend strength was 712 N/mm^2 ($46\% \cdot f_{tu}$). Two of the three beams failed in diagonal tension failure due to the rupture of the stirrups initiated at the bent part, and the remaining one failed in flexure.

- (Shehata et al. 2000)

Tests conducted by (Shehata et al. 2000) consisted on 10 beams with T-shape cross section critical to shear: 4 with CFRP stirrups, 4 with GFRP stirrups, 1 with steel stirrups and 1 without shear reinforcement. The test variables were the material properties and spacing of stirrups, and the type of flexural reinforcement (8 specimens with steel strands, 2 specimens with CFRP strands).

All beams failed in shear before yielding or rupture of the longitudinal reinforcement. In the 8 beams with FRP stirrups, shear failure was initiated by rupture of the FRP stirrups at the bent zone (6 beams) or by crushing of the concrete in the shear span (2 beams). According to the experimental results, the effective stress in the stirrups at failure was as low as 50% of the strength parallel to the fibers provided that shear failure occurs due to the rupture of the stirrups. For closely spaced stirrups, a lower contribution of the stirrups was obtained. It might be because the chance for the diagonal crack to intersect the bent zone of the stirrups is higher. (Zhao et al. 1995)

- (Bentz et al. 2010)

The experimental program conducted by (Bentz et al. 2010) consisted on 11 shear tests of FRP RC beams, 5 of them with and 6 without GFRP stirrups. The beams presented different longitudinal GFRP reinforcement ratios and different transversal GFRP reinforcement ratios.

In relation to the failure mode of the tests with stirrups, beam L05-1 failed in shear by stirrup rupture at the bottom bent zone with a maximum measured strain at mid-height of the beam of 55% the bare-bar rupture strain. Beam L05-2 failed in flexure, even though shear failure was imminent. Beam L20-1 failed by sliding along a large diagonal crack, showing the rupture of the stirrups at failure. Beam L20-2 failed in flexure by concrete crushing with the rupture of some stirrups.

One of the conclusions was that with multiple layers of longitudinal bars, the stirrups rupture did not occur at the bent location (as in beam L05-1) but near the end of the lap-splice (L20-2).



Figure 4: failure in stirrups at the bent zone of L05-1 (Bentz et al. 2010)

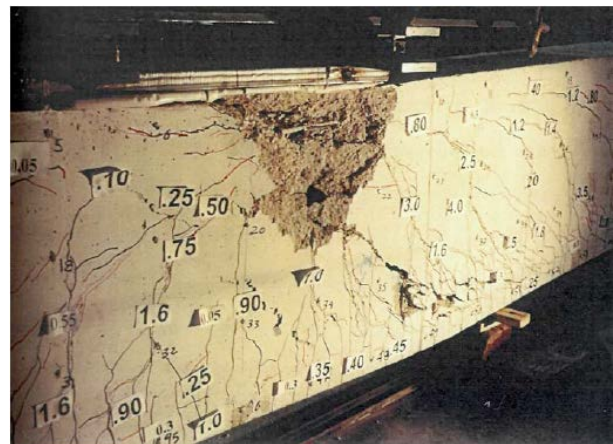


Figure 5: Flexural compression failure in constant moment region of L20-2 (Bentz et al. 2010)

- (Niewels 2008)

(Niewels 2008) carried out an experimental program with 4 concrete beams with FRP flexural and shear reinforcement tested in shear in two phases. The variables of the tests were the type of longitudinal bars and stirrups and the amount of transversal reinforcement. The beams with stirrups failed in the shear compression zone due to overstress in shear and compression. Stirrups strains above 10% were measured. However, the stirrups did not fail due to concentration of stresses at the bent zone.

- (Spadea 2010)

The experimental program of (Spadea 2010) consisted of 40 beams (8 series of 5 identical specimens) with GFRP or CFRP longitudinal and transversal reinforcement tested in a 4 point-bending configuration. Shear failure was observed in almost all tests.

In the I and III series, diagonal shear crack opened near the load application point with an inclination angle of about 70 °(Figure a). In the remaining beams, the shear crack opens at mid shear span with angles ranging between 41° and 65°. A shear failure with the critical crack closer to the load application point or at mid shear span was observed in Series I, III, V and VII (Figure b). Series II, IV, VI and VIII failed due to concrete crushing at the compression chord produced by the combined shear-flexural effect (Figure c). Figure d is represents the ultimate crushing of the concrete, which was in some beams of the IV and VIII series.

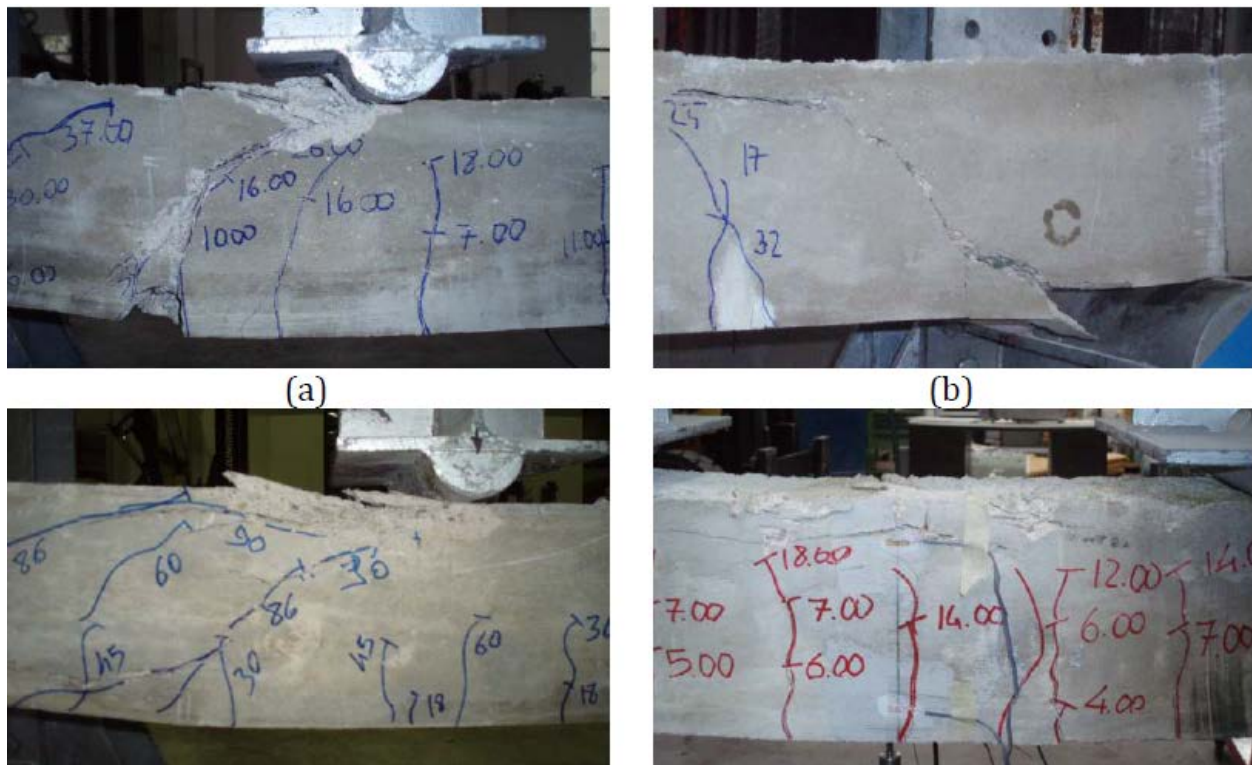


Figure 6: Types of shear failure in experimental trials(Spadea 2010)

- (Kurth 2012)

The test program made by (Kurth 2012) included 24 shear tests on 12 I-beams with three types of FRP transversal reinforcement and different ratios and two concrete classes.

The beams presented different failure modes depending on the shear reinforcement ratio; the most common one was due to shear compression (10 beams), stirrup failure (9 beams, 3 beams failed the double headed bolt of the stirrup). For the stirrups the failure occurred always in the bent zone.

This experimental campaign was deeply studied in this work by means of a numerical model. This choice was related with the quantity and quality of the information available and the relevance of the results obtained experimentally.

This work will be presented in chapter 4.

2.3 Analytical formulations for shear resistance of FRP reinforced concrete elements

Due to the specific mechanical properties of FRP reinforcement and especially their inherent lack of plasticity, FRP RC structures have a peculiar behaviour that is generally governed by brittle and undesirable modes of failure. Based on these considerations, it appears evident that both construction techniques and design philosophy need to be carefully reassessed (Pilakoutas 2000).

Therefore, in beams with longitudinal and transversal FRP reinforcement, it can be considered that the shear forces are resisted by the same mechanisms as for conventionally RC beams with steel stirrups:

- a) The shear resisted by the concrete compressed chord;
- b) The friction forces developed along the crack length, which are contrary to the relative displacement of both crack faces (aggregate interlock);
- c) The residual tensile strength existing between inclined cracks;
- d) The shear strength provided by the longitudinal reinforcement (dowel action);
- e) The shear strength provided by the transverse reinforcement (if it exists).

However, due to the lower modulus of elasticity of the FRP compared to steel, wider and deeper cracks develop, and all the shear resisting components that are related with concrete are lower in comparison to conventionally steel RC beams. Consequently, the overall shear capacity of concrete members reinforced with FRP bars is lower than that of elements reinforced with steel bars (El-Sayed & Soudki 2011).

The existing design equations of reinforced concrete beams with FRP are from:

Design guidelines:

- ACI-440.1R-06 (American Concrete Institute)
- CNR-DT 204/2006 (National Research Council –Italy)
- CSA S806-12 (Canadian Standards Association)
- JSCE 1997 (Japan Society of Civil Engineers)

Other authors:

- (Fico et al. 2008)
- (Nehdi et al. 2007)
- (Hegger et al. 2009)

According to all of them the shear strength of FRP RC structures with FRP stirrups is the sum of the concrete and the transversal FRP reinforcement contributions.

The modification of the existing code equations are based on the following approaches:

The strain approach

The fundamental principle underlying the strain approach is that, assuming perfect bond, the concrete section experiences forces and strains that are independent of the type of reinforcement utilized. Hence, if a design model using FRP reinforcement maintains the same strain as when conventional steel is used ($\epsilon_{FRP} = \epsilon_s$) and the same design forces are developed ($F_{FRP} = F_s$), then that design solution, by definition, will lead to the same safe result.

According to the strain approach, the required amount of FRP shear reinforcement is determined by limiting the maximum strain that it can develop. In some formulations, a maximum limit of 0.0025, which is the value that corresponds to the yielding strain of conventional steel bars, is suggested by (Clarke 1996). By imposing this limit, however, FRP links will only be stressed to a fraction of their potential and thus the benefits of using such materials are not taken to their maximum mechanical and economic advantage (Figure 7).

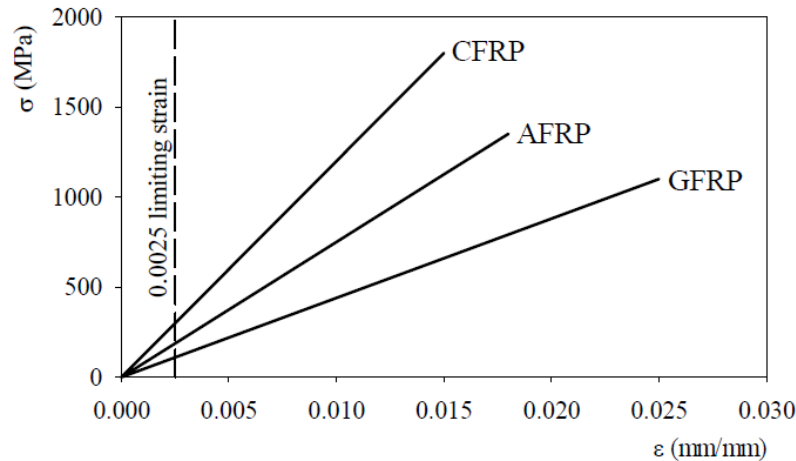


Figure 7: Limiting strain according to the Strain Approach (Clarke 1996)

The stress approach

The stress approach was developed for research purposes at the University of Sheffield (El-Ghandour et al. 1998). According to this approach, the forces derived from the strength of the materials, F_s (design force for steel) and F_{FRP} (design force for FRP), are considered to be the same, however, a restriction on the strain developed in the reinforcement is not imposed (i.e. $\epsilon_{FRP} \neq \epsilon_s$).

The shear resistance predicted by this approach is normally higher than the values obtained during testing and consequently, this formulation is only used as a research tool and it is not intended to be used for the development of design recommendations.

The modified approach

Researchers at Sheffield (El-Ghandour et al. 1999), proposed a modified version of the strain approach for the design of FRP RC flat slabs. The proposed approach was based on an experimental investigation of punching shear behaviour of FRP RC flat slabs and takes partial advantage of the force that can be developed in the FRP reinforcement when strain values beyond the strain limit imposed by the strain approach develop in the bars.

2.3.1 (ACI-440.1R-06)

The total resistance of shear beams reinforced with FRP stirrups is obtained as the sum of the concrete contribution, $V_{Rd,c}$, and the transversal FRP reinforcement, $V_{Rd,frp}$, calculated using the analogy of strut and tie:

$$V_{Rd} = V_{Rd,c} + V_{Rd,frp} \quad (2.1)$$

The contribution of the concrete resistance to shear can be calculated with the equation:

$$V_{Rd,c} = \frac{2}{5} \cdot \sqrt{f_c} \cdot b_w \cdot k \cdot d \quad (2.2)$$

Where f_c is the compressive concrete strength, b_w the web width, d the effective depth, and k is calculated as:

$$k = \sqrt{2 \cdot n_f \cdot \rho_{fl} + (n_f \cdot \rho_{fl})^2} - n_f \cdot \rho_{fl} \quad (2.3)$$

$$n_f = E_{fl} / E_c \quad (2.4)$$

E_{fl} is the modulus of elasticity of the longitudinal reinforcement and E_c is the modulus of elasticity of the concrete.

ρ_{fl} is the longitudinal reinforcement ratio that can be calculated with:

$$\rho_{fl} = \frac{A_{fl}}{b_w \cdot d} \quad (2.5)$$

Where, A_{fl} is the area of longitudinal reinforcement.

The resistance to shear provided by the transversal FRP reinforcement:

$$V_{Rd,frp} = \frac{A_{frp,v} \cdot f_{frp,v}}{s} \cdot d \quad (2.6)$$

$A_{frp,v}$ represents the amount of shear reinforcement within spacing s , $f_{frp,v}$ is the tensile strength of the transversal FRP stirrup, and d the effective depth.

The tension in the FRP reinforcement should be limited to control the depth of shear cracks and maintain the integrity of the concrete, and to prevent failure in the bent zone of the transversal reinforcement.

$$f_{frp,v} = 0.004E_{fv} \leq f_{fb} \quad (2.7)$$

Where, E_{fv} is the modulus of elasticity of the transversal FRP reinforcement and f_{fb} represents the strength of bent portion of FRP bar.

$$f_{fb} = \left(0.05 \cdot \frac{r_b}{d_b} + 0.30 \right) \cdot f_{frp,u} \quad (2.8)$$

Where r_b and d_b represents the internal radius, respectively equivalent diameter of the bent, and $f_{frp,u}$ the ultimate tensile strength of the transversal FRP stirrup.

2.3.2 (CNR-DT 204/2006)

The total shear resistance of the reinforced concrete element with FRP stirrups can be calculated with the following formula:

$$V_{Rd} = \min(V_{Rd,c} + V_{Rd,frp}; V_{Rd,cmax}) \quad (2.9)$$

Where, $V_{Rd,cmax}$ is the concrete contribution corresponding to failure due to crushing of the diagonal compression concrete strut in the web.

The contribution of the concrete resistance to shear can be calculated with the equation:

$$V_{Rd,c} = 1.3 \cdot \left(\frac{E_{fl}}{E_s} \right)^{\frac{1}{3}} \cdot \tau_{rd} \cdot k_d \cdot (1.2 + 40 \cdot \rho_{fl}) \cdot b_w \cdot d \quad 2.10$$

Where, E_s is the modulus of elasticity of the steel, and τ_{rd} is the design shear stress calculated with:

$$\tau_{rd} = 0.25 \cdot f_{ctk,0.05} \quad (2.11)$$

Where $f_{ctk,0.05}$ is the characteristic concrete tensile strength (5%fractile).

$$\rho_{fl} = \frac{A_{fl}}{b_w \cdot d} \quad (2.12)$$

k_d is a coefficient that can take the following values

- $k_d = 1.0$ in members where more than 50% of the reinforcement is interrupted;
- other cases $k_d = 1.6 - d \geq 1.0$

The resistance to shear provided by the transversal FRP reinforcement:

$$V_{Rd,frp} = \frac{A_{frp,v} \cdot f_{frp,v} \cdot d}{s} \quad (2.13)$$

$$f_{frp,v} = f_{frp,u} / \gamma_{f\phi} \quad (2.14)$$

Where $f_{frp,v}$ is the reduce tensile strength of the transversal reinforcement and $\gamma_{f\phi}$ is a partial factor to account for bending effect equal to:

- 2 when no specific experimental tests are performed
- f_{fu} / f_{bd}

Where, f_{fu} is the strength of an FRP bar and f_{bd} the design strength of the bending area of the FRP.

The maximum shear force absorbed by the diagonal compression concrete strut in the web is determined as:

$$V_{Rd,cmax} = 0.5 \cdot \nu \cdot f_c \cdot b_w \cdot 0.9 \cdot d \quad (2.15)$$

$$\nu = 0.7 - f_c / 200 \geq 0.5 \quad (2.16)$$

2.3.3 (JSCE 1997)

The total shear resistance of the reinforced concrete element with FRP stirrups can be calculated as:

$$V_{Rd} = V_{Rd,c} + V_{Rd,frp} \quad (2.17)$$

The shear resistance of concrete is:

$$V_{Rd,c} = \beta_d \cdot \beta_p \cdot \beta_n \cdot f_{vcd} \cdot b_w \cdot d \quad (2.18)$$

Where:

$$f_{vcd} = 0.2 \cdot f_c^{\frac{1}{3}} \leq 0.72 \text{ N/mm}^2 \quad (2.19)$$

$$\beta_d = \left(\frac{1000}{d} \right)^{\frac{1}{4}} \leq 1.5 \quad (2.20)$$

$$\beta_p = \left(1000 \cdot \frac{\rho_f \cdot E_f}{E_s} \right)^{\frac{1}{3}} \leq 1.5 \quad (2.21)$$

$$\beta_n = 1 \text{ (No axial forces)} \quad (2.22)$$

The shear resistance of the transversal FRP reinforcement is:

$$V_{Rd,frp} = \frac{A_{frp,v} \cdot E_{frp,v} \cdot \varepsilon_{frp,v}}{s} \cdot z \quad (2.23)$$

$$\varepsilon_{frp,v} = \sqrt{\left(\frac{h}{0.3} \right)^{\frac{1}{10}} \cdot f_c \cdot \frac{\rho_{frp} \cdot E_{frp}}{\rho_{frp,v} \cdot E_{frp,v}}} \cdot 10^{-4} \quad (2.24)$$

Where, $\varepsilon_{frp,v}$ is the design deformation of the transversal FRP reinforcement and h the height of the beam.

2.3.4 (CSA S806-12)

The total shear resistance of the reinforced concrete element with FRP stirrups can be calculated with the following formula, where the left term represents the resistance of the compressed strut.

$$V_{Rd} = V_{Rd,c} + V_{Rd,frp} \leq 0.22 \cdot f_c \cdot b_w \cdot d_v \quad (2.25)$$

The shear resistance of concrete is given by:

$$V_{Rd,c} = 0.05 \cdot \lambda \cdot \phi_c \cdot k_m \cdot k_r \cdot (f_c)^{\frac{1}{3}} \cdot b_w \cdot d_v \quad (2.26)$$

$$0.11 \cdot \sqrt{f_c} \cdot b_w \cdot d \leq V_{Rd,c} \leq 0.2 \cdot \sqrt{f_c} \cdot b_w \cdot d \quad (2.27)$$

Where:

λ is concrete density factor , equal to 1.0 for normal concrete.

ϕ_c is the concrete resistance factor

$f_c \leq 60 \text{ N/mm}^2$, is the compressive concrete strength.

$$d_v = 0.9 \cdot d \quad (2.28)$$

$$k_m = (V \cdot d / M)^{\frac{1}{2}} \quad (2.29)$$

$$k_r = 1 + (E_r \cdot \rho)^{\frac{1}{3}} \quad (2.30)$$

- If $a/d < 2.5$, $V_{Rd,c}$ shall be multiplied by k_a

$$k_a = 2.5 \cdot V \cdot d / M , \quad 1.0 \leq k_a \leq 2.5 \quad (2.31)$$

- If $d > 300$ mm and $A_t < A_{t,min}$, $V_{Rd,c}$ shall be multiplied by k_s

$$k_s = \left(\frac{750}{450 + d} \right) \leq 1.0 \quad (2.32)$$

The shear resistance of the transversal FRP reinforcement is:

$$V_{Rd,frp} = \frac{A_{frp,v} \cdot f_{frp,v} \cdot d_v \cdot \cot \theta}{s} \quad (2.33)$$

$$\theta = (30 + 7000 \cdot \varepsilon_x) \quad (2.34)$$

$$\varepsilon_x = \frac{M/d + V + 0.5 \cdot N}{2 \cdot E_f \cdot A_f} \quad (2.35)$$

$$f_{frp,v} = \min(0.005 \cdot E_{frp,v}; f_{frp,bend} = 0.4 \cdot f_{frp,u}; 1200 \text{ N/mm}^2) \quad (2.36)$$

2.3.5 Proposal by (Fico et al. 2008)

In consistency with the experimental results of (Nagasaka et al. 1933) where the average stress of FRP stirrups was only half of the breaking strength of bent portions, (Fico et al. 2008) suggested a limit strain value, $\epsilon_{f,lim}$, for the stirrups contribution depending on the fiber type, that can be observed in Table 6.

In addition, a limit of the transverse stirrups ratio of 1% was recommended for more reliable predictions.

Type of fiber	$\epsilon_{f,lim}$
CFRP	0.0035
AFRP	0.0070
GFRP	0.0085

Table 6: Limit strain value(Fico et al. 2008)

The shear resistance of the reinforce concrete element with transversal stirrups is calculated according to (CNR-DT 204/2006):

$$V_{Rd} = \min(V_{Rd,c} + V_{Rd,frp}; V_{Rd,cmax}) \quad (2.9)$$

Where $V_{Rd,c}$, $V_{Rd,frp}$ and $V_{Rd,cmax}$ are the same as in(CNR-DT 204/2006) guideline.

The formulation proposed by the (CNR-DT 204/2006) guideline for the contribution of the shear transversal FRP reinforcement $V_{Rd,frp}$ is modified to take into account the strain limitation for each type of fiber.

$$V_{Rd,frp} = \frac{A_{frp,v} \cdot f_{frp,v,u} \cdot d}{s} \cdot \frac{f_{frp,v,b}}{f_{frp,v,u}} \quad (2.37)$$

$$f_{frp,v,b} = E_{frp,v} \cdot \epsilon_{frp,lim} \quad (2.38)$$

Equation (2.37) can be rewritten as:

$$V_{Rd,frp} = \frac{A_{frp,v} \cdot \epsilon_{f,lim} \cdot E_{frp,v} \cdot d}{s} \quad (2.39)$$

2.3.6 Proposal by (Nehdi et al. 2007)

The total shear resistance of the reinforced concrete element with FRP stirrups is given by:

$$V_{Rd} = V_{Rd,c} + V_{Rd,frp}$$

The shear resistance of concrete depends on the a/d relation, where a is the shear span.

- For $a/d > 2.5$:

$$V_{Rd,ct} = 2.1 \cdot \left(\frac{f_c \cdot \rho \cdot d}{a} \cdot \frac{E_f}{E_s} \right)^{0.3} \quad (2.40)$$

- For $a/d < 2.5$:

$$V_{Rd,ct} = 2.1 \cdot \left(\frac{f_c \cdot \rho \cdot d}{a} \cdot \frac{E_f}{E_s} \right)^{0.3} \cdot \frac{2.5d}{a} \quad (2.41)$$

The shear resistance of the transversal FRP reinforcement:

$$V_{Rd,frp} = 0.5 \cdot (A_{frp,v} \cdot f_{frp,v,u})^{0.5} \cdot b_w \cdot d \quad (2.42)$$

2.3.7 Proposal by (Hegger et al. 2009)

(Hegger et al. 2009) developed a shear design equation where the concrete shear strength contribution is based on Eurocode and the contribution of FRP shear reinforcement depends on a strain limit obtained from existing experimental work.

The total shear resistance of the reinforced concrete element with FRP stirrups:

$$V_{Rd} = V_{Rd,c} + V_{Rd,frp}$$

The shear resistance of concrete:

$$V_{Rd,c} = k_f \cdot \beta \cdot 0.205 \cdot \kappa \cdot \left(100 \cdot \rho \cdot \frac{E_r}{E_s} \cdot f_{ck} \right)^{\frac{1}{3}} \cdot b_w \cdot d \quad (2.43)$$

$$k_f = 1 - 10 \cdot \rho_{frp,v} \cdot \frac{E_{frp,v}}{E_c} \quad (2.44)$$

$$\beta = 3 \cdot d/a \quad (2.45)$$

$$\kappa = 1 + \sqrt{200/d} \quad (2.46)$$

Where:

β factor that increases the shear strength of the concrete near the supports.

The shear resistance of the transversal FRP reinforcement:

$$V_{Rd,frp} = \min \left(\frac{A_{frp,v} \cdot f_{frp,v} \cdot z \cdot \cot \theta}{s}; b_w \cdot z \cdot \alpha_c \cdot f_{cm} \cdot \frac{1}{\cot \theta + \tan \theta} \right) \quad (2.47)$$

$$z = 0.9d \quad (2.48)$$

$$f_{frp,v} = \min (0.4 \cdot f_{frp,u}; E_{frp,v} \cdot \varepsilon_{frp,v,lim}) \quad (2.49)$$

$$\varepsilon_{frp,v,lim} = 3 + 0.015 / \left(\rho_{frp,v} \cdot E_{frp,v} / E_c \right)^{0/00} \quad (2.50)$$

Where:

$\alpha_c = 0.2$

θ is the truss angle

$f_{frp,u}$ is the ultimate tensile strength of FRP

$f_{frp,v}$ is the design value of the tensile strength of FRP reinforcement

3 Non-linear shear-sensitive fiber beam model

The present work used the program CONSHEAR to analyze the behaviour of the beams tested by (Kurth 2012).

CONSHEAR (Ferreira 2013) is a computer program for the nonlinear analysis of reinforced and prestressed concrete frame structures by means of the fiber beam element approach and accounting for axial force-shear-bending interaction. The numerical model implemented in CONSHEAR is based on a previous model founded on the Finite Element Method (FEM) and on the Bernoulli's beam theory that is implemented in the computer program CONS (Marí 2000).

In general, its main characteristics are: the Timoshenko beam theory is assumed at the element level; a hybrid sectional formulation, in which input variables comprises both kinematical and force quantities, links the plane section theory with the assumption of a constant shear stress flow. The multiaxial constitutive behaviour of concrete is assumed through a smeared crack approach with full rotating cracks; compression weakening (softening) and tensile tension stiffening effects are included. Longitudinal reinforcement is simulated through the use of steel filaments while transversal reinforcement is considered smeared in the concrete fibers.

In the following, a brief insight into the fundamental of the numerical model that is implemented into the computer code CONSHEAR is offered.

3.1.1 Structural scheme

In numerical simulations by means of the FEM using 1D fiber beam models the structure is divided into elements interconnected by nodes and the material nonlinearities are introduced at each control section that is discretized into longitudinal fiber as observed in Figure 8.

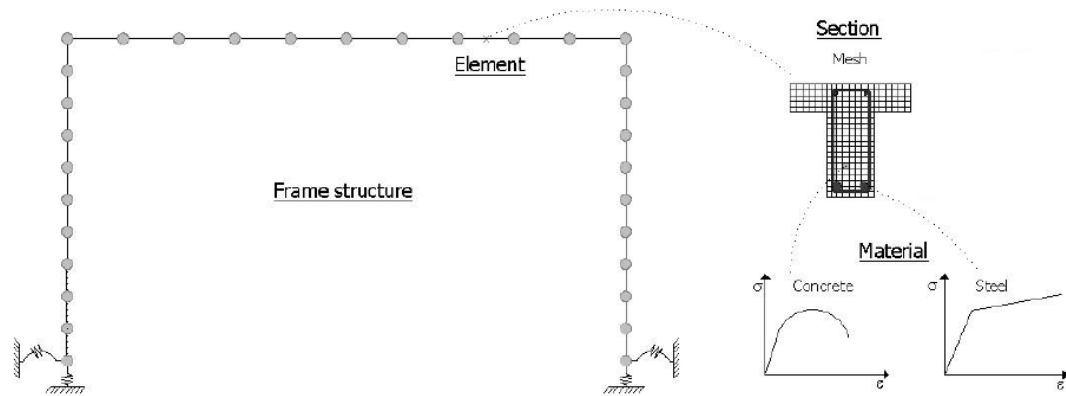


Figure 8: General characteristics of the fiber beam models (Ferreira 2013)

3.1.2 Finite element

A 2-noded Timoshenko finite element with linear shape functions is used in the model.

For the 2D case, the displacement field is a function of two displacements, axial u and vertical w , and a rotation θ_y . In the Timoshenko beam theory it is assumed that undeformed plane sections perpendicular to the beam axis remain plane but not necessarily normal to the longitudinal axis after deformation. An average rotation of the section due to distortion is considered in order to maintain valid the plane section assumption.

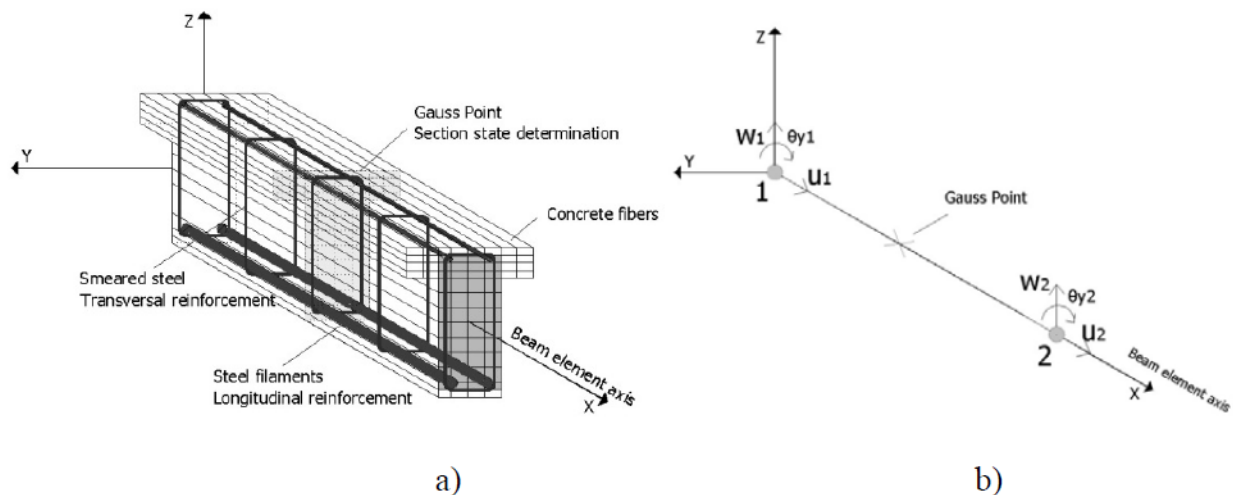


Figure 9: Fiber beam model in CONSHEAR: a) general characteristics b) finite element for the 2D case (Ferreira 2013)

3.1.3 Sectional level

The cross-section is discretized into two types of fibers, as presented in Figure 3: the non-shear resistant ones, submitted to 1D axial stresses only, and the shear resistant fibers, submitted to a multiaxial stress-strain state. Axial force and bending moment are resisted by the entire cross-section; shear forces and interaction with normal forces are only considered in the shear resistant fibers.

This fiber subdivision is an input of the model related to the shape of the cross section: for rectangular, T-shape and I-shape, the fibers that pertain to the web (disregarding the bottom cover area) are considered shear resistant. Particularly for the T-shape and I-shapes cross sections, if there is strong evidence that compressive flanges contribute to the shear-resistance mechanism, an effective area of the flange b_{eff} determined according to (Zararis et al. 2006) can be considered as 2D fibers.

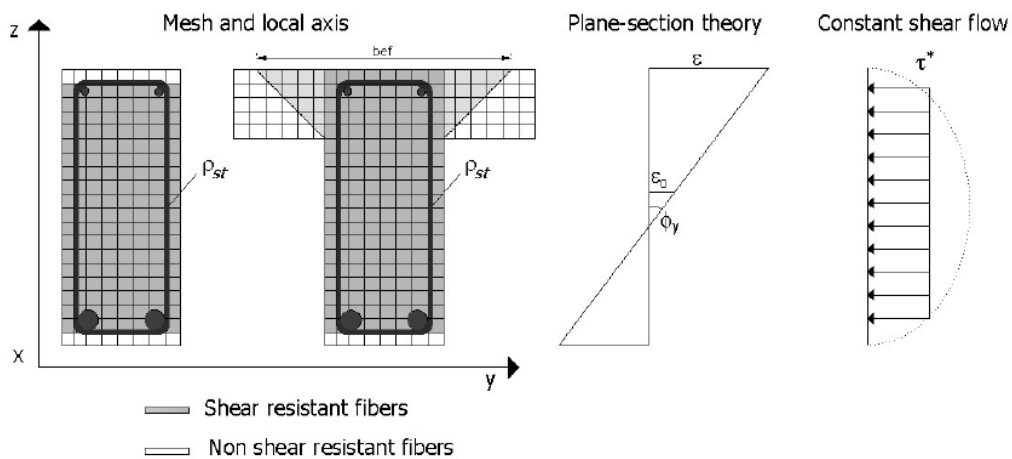


Figure 10: Assumptions of the model at the section level (Ferreira 2013)

3.1.4 Material models

Cracked concrete is assumed as a homogeneous material with orthotropic behaviour (Figure 11(a)). The constitutive model is formulated in terms of average principal strains $\epsilon_{12} = [\epsilon_1 \ \epsilon_2]^T$ and stresses $\sigma_{12} = [\sigma_1 \ \sigma_2]^T$ between the undamaged and cracked areas. . In this formulation

subscripts “1” and “2” denote the maximum and minimum principal strains and stresses, respectively.

The equation considered for concrete in compression is presented in Figure 11(b): ϵ_p is the strain at peak stress f_p and ϵ_{p2} is the plastic strain after unloading by means of the initial stiffness E_0 . For concrete in tension (Figure 11(c)) a linear response is considered before cracking and remaining stresses in the cracked stage: f_t and ϵ_{cr} are respectively the maximum tensile stress and strain of concrete for which cracking appears. After cracking tensile softening is represented by (Cervenka 1985) curve

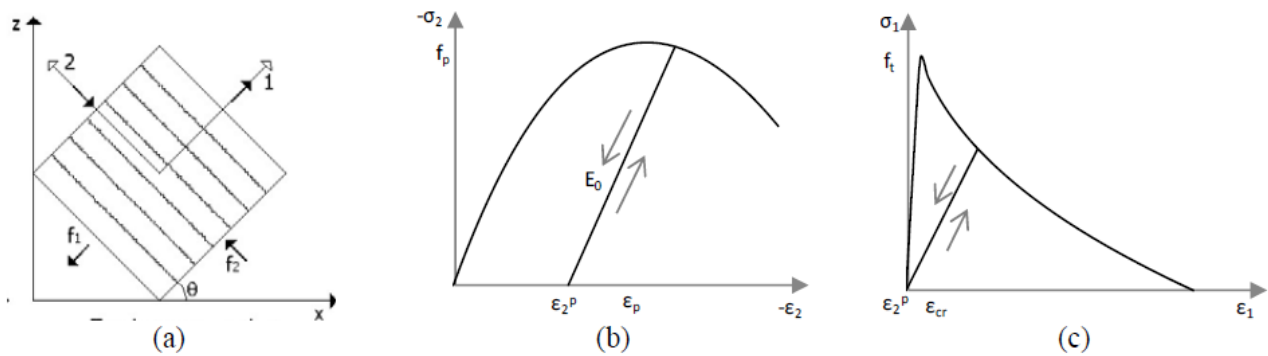


Figure 11: Constitutive model for the concrete: (a) smeared crack, (b) compression, (c) tension (Ferreira 2013)

Longitudinal (passive) and transversal (passive or active) reinforcements are considered under 1D stress-strain states by means of a bilinear uniaxial constitutive equation with kinematic hardening (Figure 12): f_{sy} and ϵ_{sy} correspond to the yielding strength and strain and f_{su} and ϵ_{su} to the ultimate strength and strain of the reinforcement material (e.g. steel, FRP, etc.)

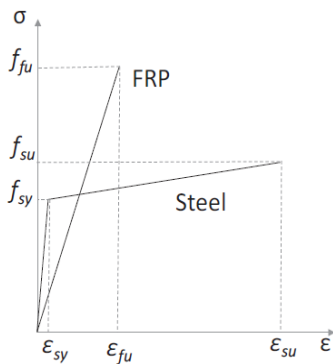


Figure 12: Constitutive model for the reinforcement (Ferreira 2013)

3.1.5 Representation of cracks

Cracking patterns are graphically represented in post-process by means of an external algorithm written in MATLAB. As at each Gauss point the principal strains and directions are known (they are outputs of the numerical model), when the principle tensile strain in each fiber reaches the critical strain ($\epsilon_1 > \epsilon_{cr}$), an orthogonal line with the inclination of the correspondent principal direction is printed.

Due to the non-verticality of the cracks, the information of the strain state in the location of the crack path does not correspond to a single Gauss point. Consequently, as schematically represented in Figure 13, the strain state corresponding to the location of a crack is obtained using a linear interpolation between the strain states of the two close-most Gauss points.

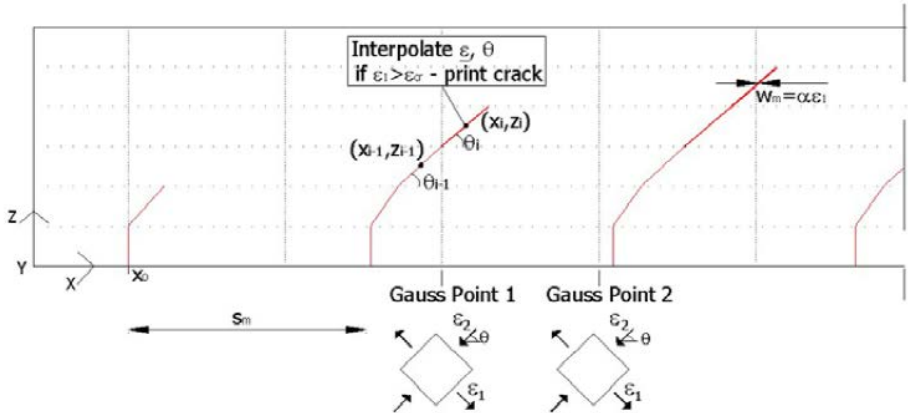


Figure 13: Scheme of the post-processing method for the representation of the cracks (Ferreira 2013)

4 Numerical analysis of FRP RC beams

4.1 Description of the experimental campaign

4.1.1 General

The test program made by (Kurth 2012) included 24 shear tests on 12 I-beams with three types of FRP Shear reinforcement and different reinforcement ratio and two concrete classes.

One of the objectives of this experimental study was to determine the shear resistance of the reinforced specimens with FRP and the failure location in the stirrups.

The beams presented 3 different failure modes depending on the shear reinforcement ratio: i) diagonal tension failure, ii) rupture of the shear reinforcement or iii) web crushing failure of concrete. Stirrups failure always occurred at the bent zone because the tensile strength there is significantly reduced due to the bending of the FRP bars into stirrup configuration.

Figure 14 represents one of the studied specimens.

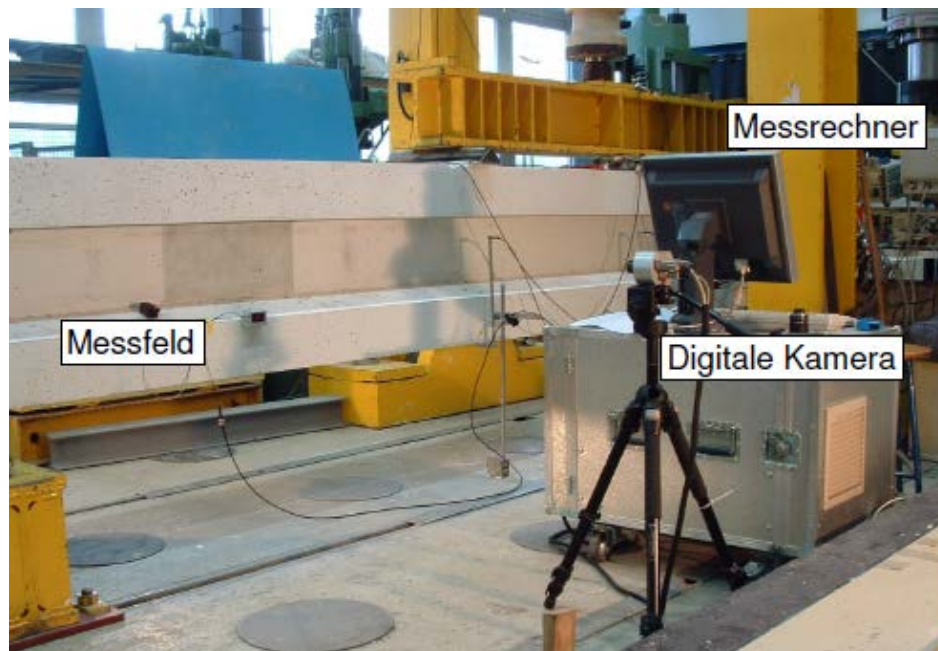


Figure 14: Experimental tests on the beam (Kurth 2012)

4.1.2 Materials

All the beams are reinforced with Fiberglass plastics (FRP) both longitudinal and transversally.

As longitudinal reinforcement, there were two different Rod types (type I and II). The nominal diameter of the bending reinforcement was $d_f = 32$ mm. Bars with the nominal diameter $d_f = 16$ mm served as structural reinforcement for fixing the stirrup in the pressure zone.

There was no data available on experimental tensile testes for determining the mechanical properties of the longitudinal reinforcement ; hence, the elastic modules and tensile strengths were considered the same as in preliminary experiments (Niewels 2008) in the numerical model. The properties of the longitudinal reinforcement are listed in Table 7.

As shear reinforcement, there were three different types (A, B and C). Types A and B had a nominal diameter of $d_f = 12$ mm. The shear reinforcement type C consisted of a straight FRP rod $d_f = 16$ mm and at its extremities are connected with double-headed bolts (DHB). The properties of the transversal reinforcement are listed in Table 8.

The FRP reinforcement were provided by three manufacturers. The longitudinal reinforcement type I and the shear reinforcement type A are products of a manufacturer. The reinforcement types II, B and C are produced by a second manufacturer.

The concrete strength classes are C30 / 37 and C60 / 75. The cube compressive strength f_{cm} , cylinder compressive strength f_{cm} , the concrete tensile strength f_{ctm} , and the modulus of elasticity E_{cm} were measured on cubes with an edge length of 150 mm and cylinders with the height of 300 mm and a diameter of 150 mm determined on each test day.

Reinforcement	Diameter d_f [mm]	Modulus of elasticity [N/mm ²]	Tensile Strength E_{fi} f_{fi} [N/mm ²]
Typ I	32	59000 ¹⁾	1124 ¹⁾
Type II	32	62600 ²⁾	>1000 ³⁾

1) Preliminary; 2) /Niewels08/; 3) Manufacturer specifications

Table 7: Characteristics of longitudinal reinforcement (Kurth 2012)

Reinforcement	Diameter df[mm]	Modulus of elasticity Efl [N/mm ²]	Tensile Strength ffl [N/mm ²]
Typ A	12	56200	382
Typ B	12	57000	770
Typ C	16	63400	611

Table 8: Characteristics of transversal reinforcement (Kurth 2012)

4.1.3 Geometry

The beams have an I-shape cross-section with a 10 cm narrow web, length of 7.0 m with 3 sections that have different reinforcement percentages.

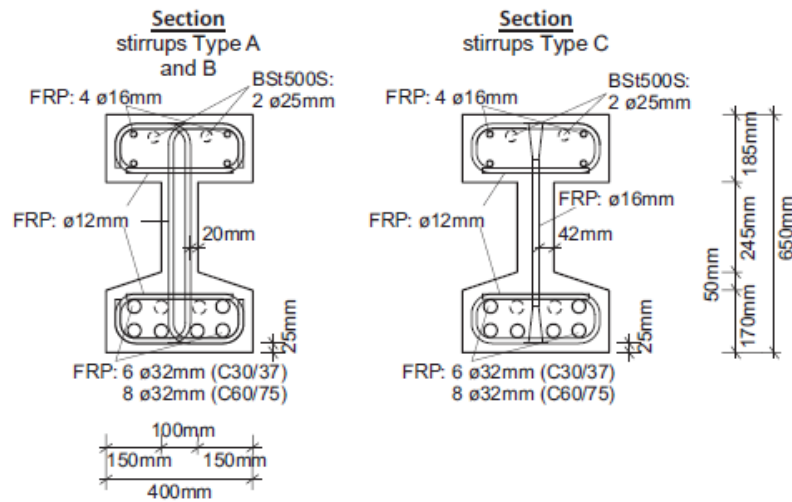
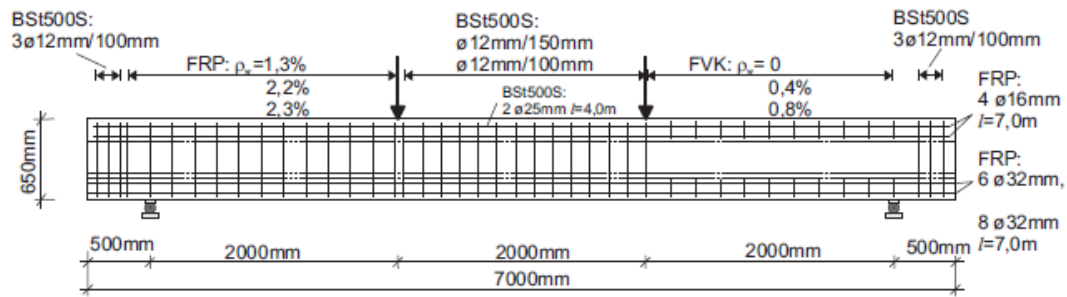
Each beam was tested in twice, in different setups. The right-span of the beam has a lower shear reinforcement percentage provided or no shear reinforcement at all. The left-span is highly reinforced. In the central portion where a bending failure should be excluded, steel reinforcement BST500 was used.

For longitudinal reinforcement was used six or eight $\varnothing 32$ mm FRP ($\rho_l=8.5\%$ and 11.5%), for the bending critical zone were additionally provided two BST500 $\varnothing 25$ mm rebar rods.

As shear reinforcement the reinforcement types A, B and C were used, and two small closed stirrups along the perimeter of the section and tension zone.

4Figure 15 shows the distribution of longitudinal and transversal reinforcement and

Figure 16 shows the type of stirrups used in the different beams.



4Figure 15: Reinforcement drawing (Kurth 2012)

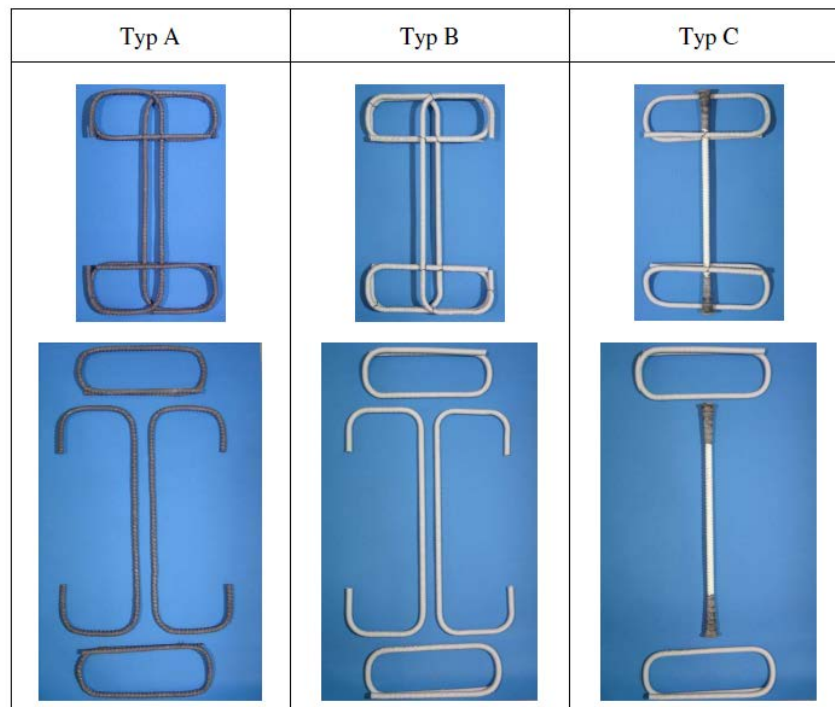


Figure 16: Type of stirrups (Kurth 2012)

4.1.4 Experimental setup for shear tests

The experimental setup is illustrated in Figure 17.

Two shear tests were performed per specimen with different load and support positions.

The first part of the experiment is a 4-point bending test; the failure was produced on the right side where the weaker shear reinforcement (or no shear reinforcement) is located.

The second part of the experiment was a 3-point bending test. Here, failure occurred in the left part of the beam that was higher transversally reinforced.

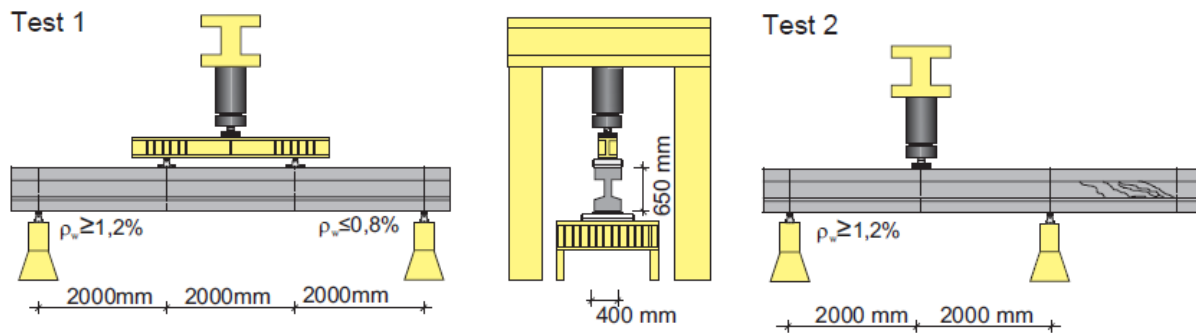


Figure 17: Experimental set-up of shear tests (Kurth 2012)

The load was applied to about 50% of the loading cell capacity and controlled with 5 kN / min and 10 kN / min and the displacement controlled at 0.5 mm / min and 1.0 mm / min.

The tests were stopped four to seven times, at constant load or constant deformation, to carry out crack width measurements.

The following sensors were used to record the experimental data and its position can be seen in Figure 14.

- Concrete longitudinal strains in compression (strain gages = DMS) B1 ... B14
- longitudinal strains in concrete in the tension / compression zone (transducer) D1 ... D3
- reinforcement slip on the beam ends (sensor) E1 and E2

- Strains in concrete in the shear field (transducer Rosette) R1 ... R6
- shear crack width (sensor) S1 S2 ...
- displacements (displacement transducer) W1 W5 ...
- strains in the longitudinal reinforcement (DMS) LG1 ... LG7
- strains in the shear reinforcement (DMS) SG1 ... SG30

The basic arrangement of the metrological devices for concrete are in Figure 18 and for reinforcement are in Figure 19

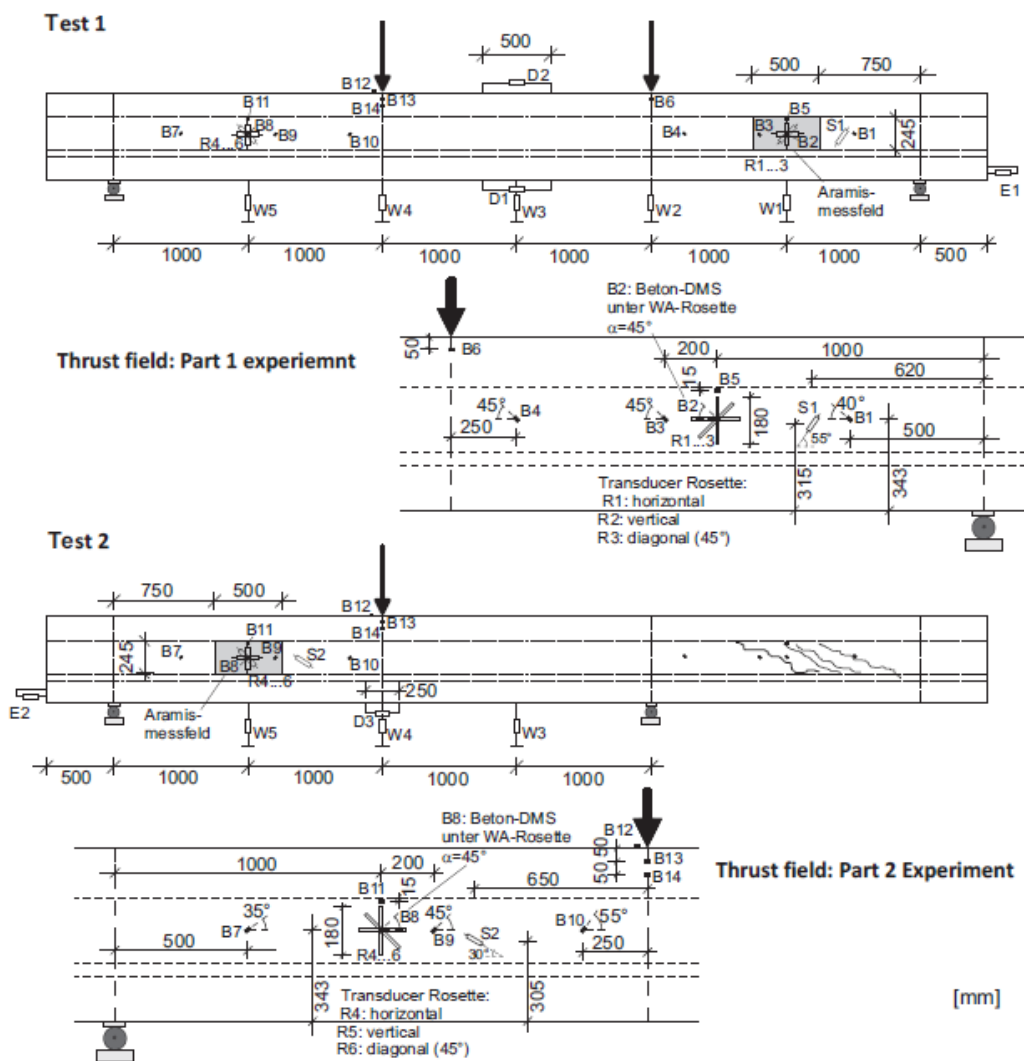


Figure 18: Metrology of concrete (Kurth 2012)

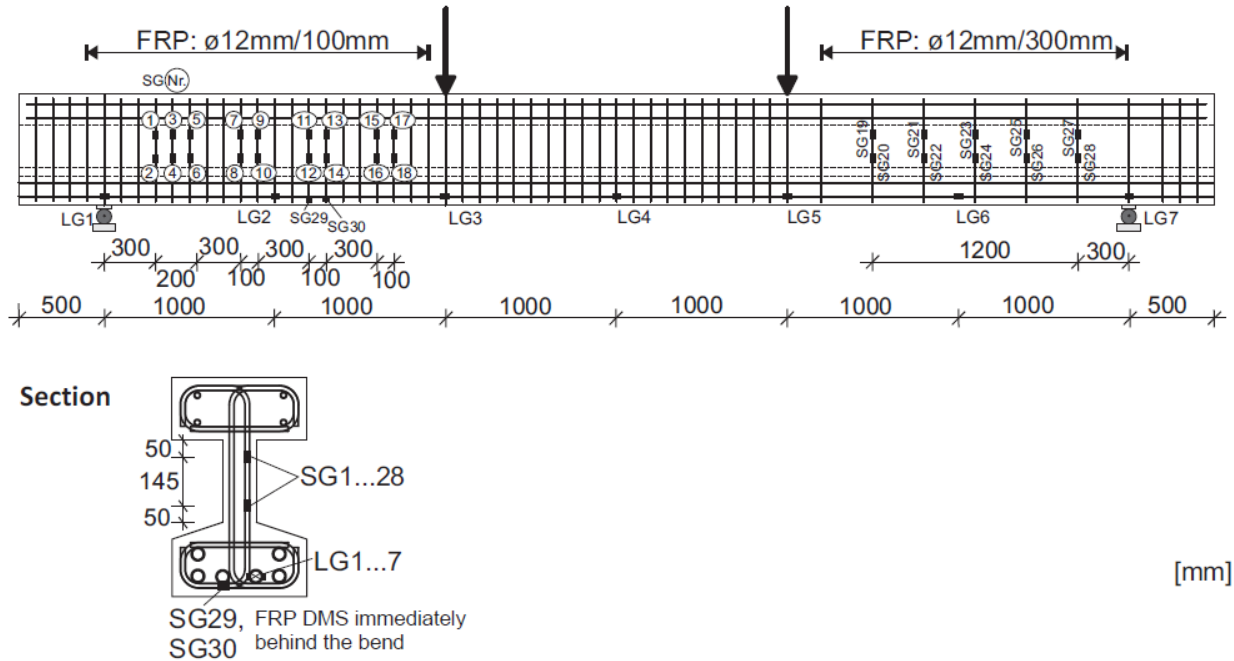


Figure 19: Metrology of reinforcement (Kurth 2012)

4.1.5 Failure modes

Stirrup failure

The specimens with lower shear reinforcement ratios ($\rho_w = 0.45$ and 0.75%) and medium shear reinforcement ratios ($\rho_w = 1.26\%$) and for high concrete strengths ($f_{cm} = 75.7$ and 82.0 N/mm^2) presented failure of the transversal reinforcement, due to a combined shear-tensile stress locally present in the region of the main shear crack (Figure 20).



Figure 20: Cracking at failure in experimental S4AH-0.8-7 ($r_w = 0.75\%$, $f_{cm} = 42.2 \text{ N/mm}^2$) (Kurth 2012)

Figure 21 shows the damaged stirrups types A and B after the failure in the test S4AH-0.8-7 and S6BN-0.8-11. In contrast, the reinforcement type C presented a local failure in the connections as the FRP rod was pulled out of the polymer concrete anchor head (Figure 22).

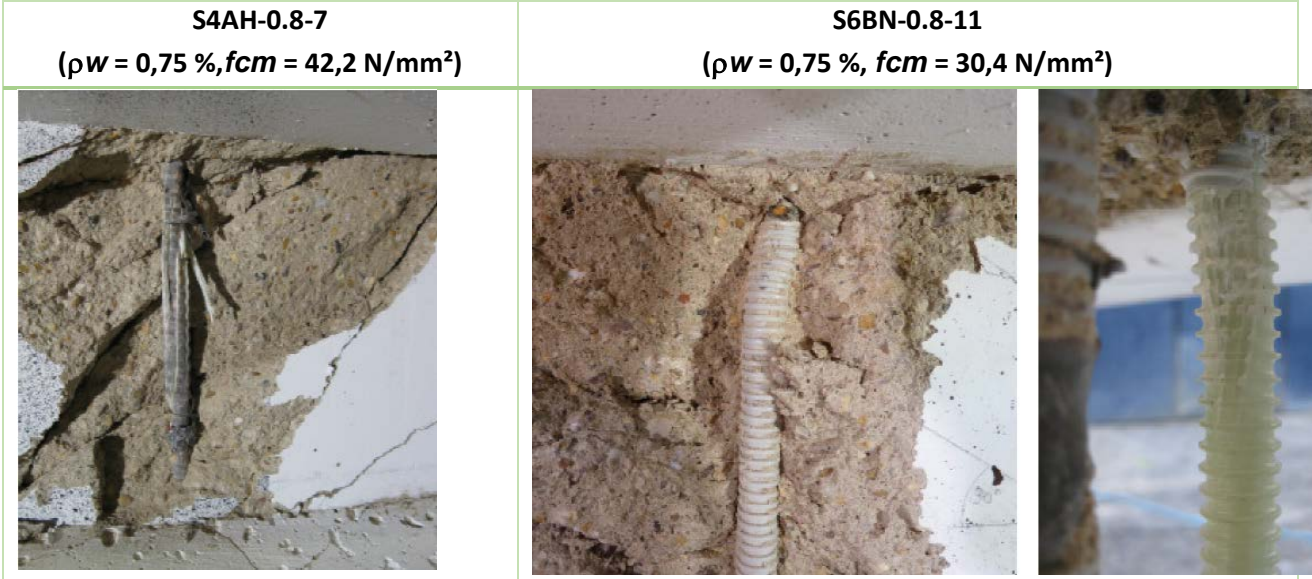


Figure 21: Damaged stirrups (Type A and B) after failure in experiments with a shear reinforcement degrees ρ_w of 0.75% (Kurth 2012)

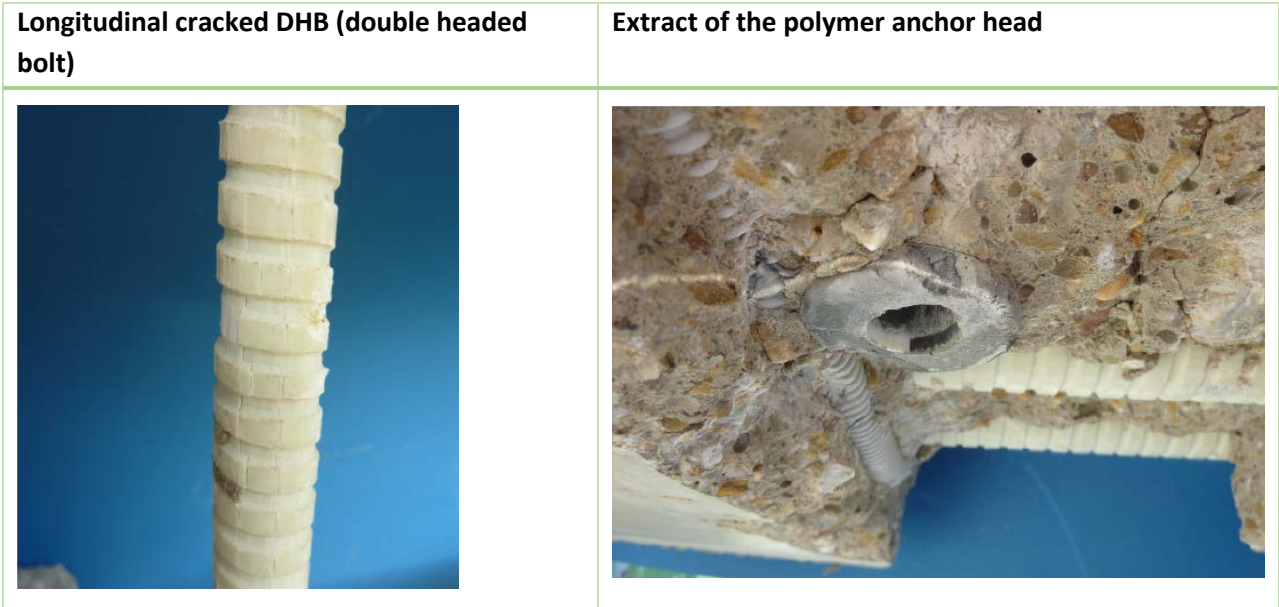


Figure 22: Damaged double headed bolt (type C) after failure while trying S12CH-0.7-23 ($\rho_w = 0.75\%$, $f_{cm} = 73.1 \text{ N/mm}^2$)(Kurth 2012)

Diagonal compression failure

In the experiments with high shear reinforcement ratios, from $\rho_w = 2.22\%$ to $\rho_w = 2.26\%$, and medium shear reinforcement degrees ($\rho_w = 1.26\%$) with the lower concrete strengths ($f_{cm} \leq 73.1 \text{ N/mm}^2$) failure occurred by crushing of concrete in the web (diagonal compression shear failure)



Figure 23: Cracking at failure in experimental S6BN-2.3-12 ($\rho_w = 2.26\%$, $f_{cm} = 30.7 \text{ N/mm}^2$)(Kurth 2012)



Figure 24: Cracking at failure in experimental S2AN-2.3-4 ($\rho_w = 2.26\%$, $f_{cm} = 33.5 \text{ N/mm}^2$)(Kurth 2012)

When compression struts fail different failure images were observed. In Experiments S2AN-2.3-4 and 2.3-8-S6BN-2.3-12 was almost completely blown off the concrete cover in the web area at failure of the concrete strut (Figure 24).

In Table 9 are presented, for each specimen, the different types of failure along with the transversal reinforcement ratio ρ_w , concrete strength f_{cm} , average shear crack angle at failure β_r and the ultimate shear force V_u .

Test	ρ_w [%]	f_{cm} [N/mm ²]	β_r [°]	V_u [kN]	Failure type
S1AN-1.3-2	1,20	38,4	40	427	diagonal tension failure
S2AN-0.8-3	0,75	34,1	30	332	stirrup failure
S2AN-2.3-4	2,26	33,5	36	486	diagonal tension failure
S3AH-1.3-6	1,26	82,0	31	571	stirrup failure
S4AN-0.8-7	0,75	42,2	32	326	stirrup failure
S4AH-2.3-8	2,26	42,6	34	544	diagonal tension failure
S5BN-1.3-10	1,26	42,8	37	439	diagonal tension failure
S6BN-0.8-11	0,75	30,4	33	302	stirrup failure
S6BN-2.3-12	2,26	30,7	37	448	diagonal tension failure
S7BH-1.3-14	1,26	75,7	31	626	stirrup failure
S8BH-0.8-15	0,75	72,7	27	439	stirrup failure
S8BH-2.3-16	2,26	69,9	33	581	diagonal tension failure
S9CN-1.3-18	1,26	37,7	36	410	diagonal tension failure
S10CN-0.7-19	0,75	32,0	23	304	failure of DHB head
S10CN-2.2-20	2,22	33,6	34	484	diagonal tension failure
S11CH-0.4-21	0,45	67,6	28	374	failure of DHB head
S11CH-1.3-22	1,26	71,0	33	621	diagonal tension failure
S12CH-0.7-23	0,75	73,1	32	441	failure of DHB head
S12CH-2.2-24	2,22	73,9	36	742	diagonal tension failure

Table 9: Types of failure for the experimental beams

In the present work, 5 beams were considered to be simulated with CONSHEAR S2AN-0.8-3, S4AH-0.8-7, S6BN-0.8-11, S8BH-0.8-15, S10CN-0.7-19 - that are loaded in 2-point bending configuration, in the first phase of testing

This choice was motivated by the fact that the second test is influenced by the damage brought from the first test, which could only be well captured by a phased analysis, which is out of the aims of this work. Also, experimental data from test 1 are more reliable to be compared with the numerical results, as they are less influenced by the previous testing and consequent damage.

Table 10 lists the characteristics of the beams under study. The dimensions are the same for all the beams, 3 beams (S2AN-0.8-3, S6BN-0.8-11 and S10CN-0.7-19) are reinforced with 6 ϕ 32 mm FRP, having the longitudinal ratio ρ_l of 8.5% and 2 with 8 ϕ 32 (S4AH-0.8-7 and S8BH-0.8-15) having the longitudinal ratio ρ_l of 11.5%. For transversal reinforcement there are 3 types of stirrups used with 2 different diameters ϕ 12 (S2AN-0.8-3, S4AH-0.8-7, S6BN-0.8-11, S8BH-0.8-15) and ϕ 16 (S10CN-0.7-19).

Trial	Type reinf	b [mm]	b _w [mm]	h [mm]	E _c [N/mm ²]	f _{cm} [N/mm ²]	f _{ctm} [N/mm ²]	Ø/s [mm]	ρ _w [%]	E _{fw} [N/mm ²]	f _{fw,exp} [N/mm ²]	ε _{u,t}	ρ _l [%]	E _{fl} [N/mm ²]	f _{fl} [N/mm ²]	ε _{u,l}
S2AN-0.8-3	A, I	400	100	650	25600	34	2,70	Ø12/ 300	0,75	56200	382	0.0068	8,52	59000	1000	0.017
S4AH-0.8-7	A, I	400	100	650	25500	42	2,31	Ø12/ 300	0,75	56200	382	0.0068	11,57	59000	1000	0.017
S6BN-0.8-11	B, II	400	100	650	24600	30	2,32	Ø12/ 300	0,75	57000	770	0.0135	8,44	62600	1000	0.016
S8BH-0.8-15	B, II	400	100	650	33400	73	3,56	Ø12/ 300	0,75	57000	770	0.0135	11,47	62600	1000	0.016
S10CN-0.7-19	C, II	400	100	650	23200	32	2,20	Ø16/ 270	0,74	63400	611	0.0096	8,44	62600	1000	0.016

Table 10: Beam dimensions, concrete properties, longitudinal reinforcement, and transversal reinforcement (Kurth 2012)

4.2 Numerical model

The first objective of the numerical analysis is the validation of the computer program for the case of FRP RC beams by comparing the numerical results with the experimental data captured in local points by the sensors. After validating the model, the second objective is to perform a deeper analysis of the structural behaviour of the beams.

The following sensors were considered to perform the comparison with the numerical outputs: for the concrete strain compression (B4-right side of the beam);, displacement transducer (W3-middle of the beam); strain in the longitudinal reinforcement (LG1, LG2, LG3 ,LG4 ,LG5 ,LG6 ,LG7); strain in the shear reinforcement (SG17...SG26- right side of the beam) and shear crack width (S1 – right side of the beam) . This was all the data available in the original reference by (Kurth 2012) .

Since the numerical model is based on the finite element method, it is necessary to discretize the beam to be analyzed into a mesh. As shown in Figure 27, the beam was simulated using 28 bar type elements of equal length, generating 29 nodes. Nodes 3 and 27 correspond to the simply supported points, while the node 15 coincides with the center-beam section. In turn, the cross section has been divided into 8 trapeziums that are discretized into filaments as observed in Figure 25(Ferreira 2013).

Longitudinal rebars were modeled in their real position in the cross-section. Furthermore in Figure 26, it is considered a shear resistant zone that is composed of the web and the effective width of the flange ($b_{eff}=340\text{mm}$) which was calculated using the formulas in (Zararis et al. 2006).

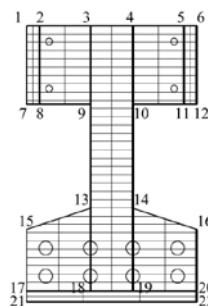


Figure 25: Discretization of the cross section

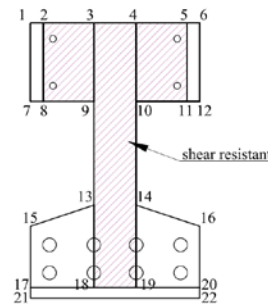


Figure 26: Shear resistant zone

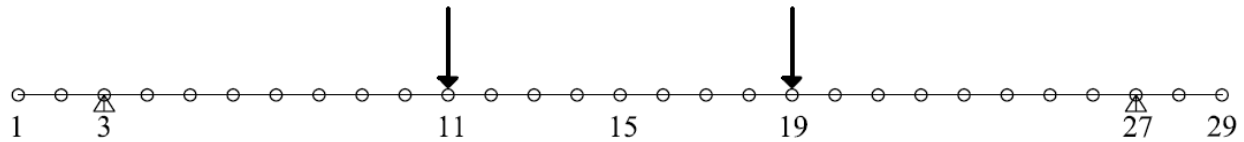


Figure 27: Discretization of the beam

The model with CONSHEAR is the same for all the beams since they have the same length $L=7$ m and same cross-section dimensions $b=400$ mm, $b_w=100$ mm, $h=650$ mm.

The difference between the beams are only related with the reinforcement configurations, as can be observed in Figure 28 for longitudinal reinforcement and in Figure 29 for transversal reinforcement.

The specimens S2AN-0.8-3 and S4AH-0.8-7 have the same transversal reinforcement ($\phi 12$ FRP at a pace of 300 mm) on the right side of the beam and a tensile strength of $f_{fw}= 382$ N/mm². The difference between them is the longitudinal reinforcement- S2AN-0.8-3 has 6 $\phi 32$ while S4AH-0.8-7 has 8 $\phi 32$ both have an elastic modulus of $E_{fi}= 5900$ N/mm². Also the concrete characteristics differ; S2AN-0.8-3 has a compressive strength of $f_{cm}=34$ N/mm² and S4AH-0.8-7 of $f_{cm}=42$ N/mm².

The specimens S6BN-0.8-11 and S8BH-0.8-15 are reinforced transversally with $\phi 12$ FRP at a pace of 300 mm with a tensile strength of $f_{fw}= 770$ N/mm². Longitudinally S6BN-0.8-11 is reinforced with 6 $\phi 32$ and S8BH-0.8-15 with 8 $\phi 32$, both with elastic modulus of $E_{fi}=62600$ N/mm². The compressive strength of concrete is of $f_{cm}=30$ N/mm² for S6BN-0.8-11 and of $f_{cm}=73$ N/mm² for S8BH-0.8-15.

Beam test S10CN-0.7-19 is reinforced transversally with $\phi 16$ FRP at a pace of 270 mm with a tensile strength of $f_{fw}=611$ N/mm²; the longitudinal reinforcement is of 6 $\phi 32$ with an elastic modulus of $E_{fi}=62600$ N/mm²; the strength of concrete is $f_{cm}=32$ N/mm².

The specimen S6BN-0.8-11 is compared in detail with the experimental results and discussed deeply in the following section, as it presents the best fitting with the experimental data. The results of the other simulated beams are treated with less detail and presented in a separate section at the end of the present chapter.

Test	Longitudinal reinforcement	Transversal reinforcement	
S2AN-0.8-3 S4AH-0.8-7		Section 1-1 	Section 2-2
		Section 1-1 	Section 2-2
S10CN-0.7-19		Section 1-1 	Section 2-2

Figure 28: Longitudinal and transversal reinforcement of the test beams(Kurth 2012)

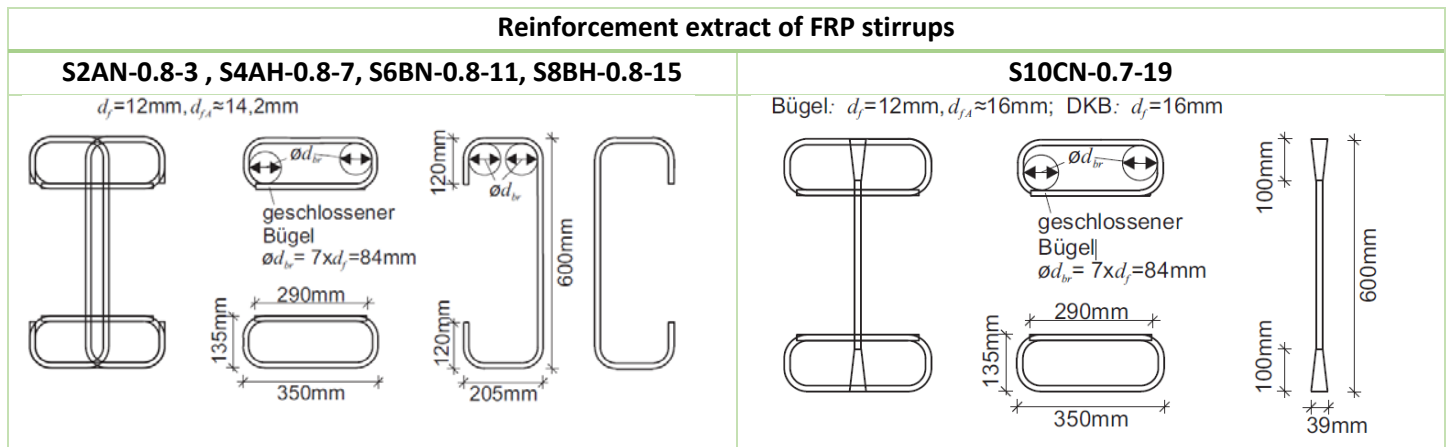


Figure 29: FRP stirrups configurations (Kurth 2012)

4.3 Comparison of numerical and experimental results

4.3.1 Test beam: S6BN-0.8-11

In the experimental test, the total load applied to the beam is 604 kN, corresponding to a shear force of 302 kN.

In the modeling in order to resemble the mode of application of the load and also to observe the nonlinear behaviour of the beam throughout the experiment, 100 load steps with a load step increment of 1 kN and 0.5 kN were used. The lower loading step of 0.5 kN is applied to higher load levels near failure to determine the breaking load more accurately.

Figure 30 shows the plan of reinforcement and Figure 31 shows the 2 different cross-sections of the beam.

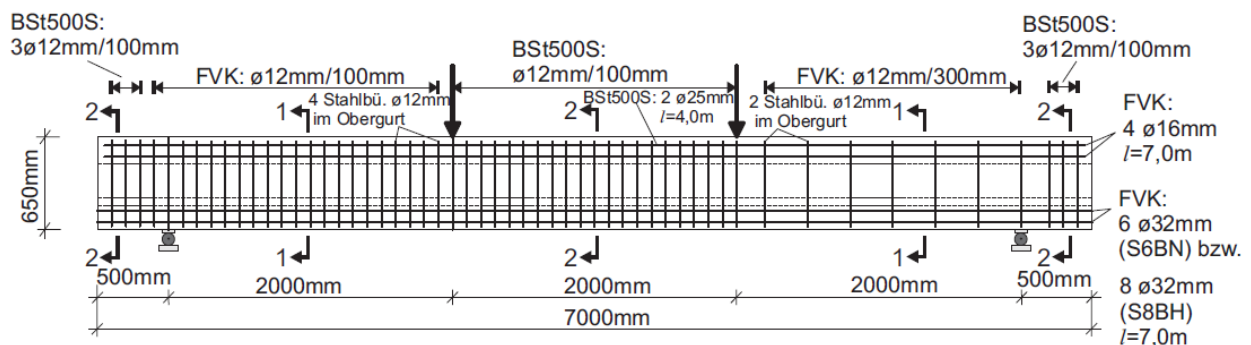


Figure 30: Plan of reinforcement for test beam: S6BN-0.8-11(Kurth 2012)

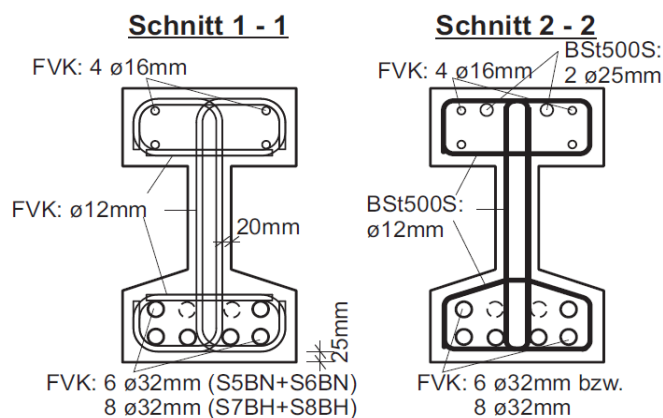


Figure 31: Beam cross-sections for test beam: S6BN-0.8-11(Kurth 2012)

In Figure 32 and Figure 33 the sensors used for comparison with the numerical results are highlighted; this includes data from strains in concrete, FRP longitudinal reinforcement, and FRP transversal reinforcement FRP.

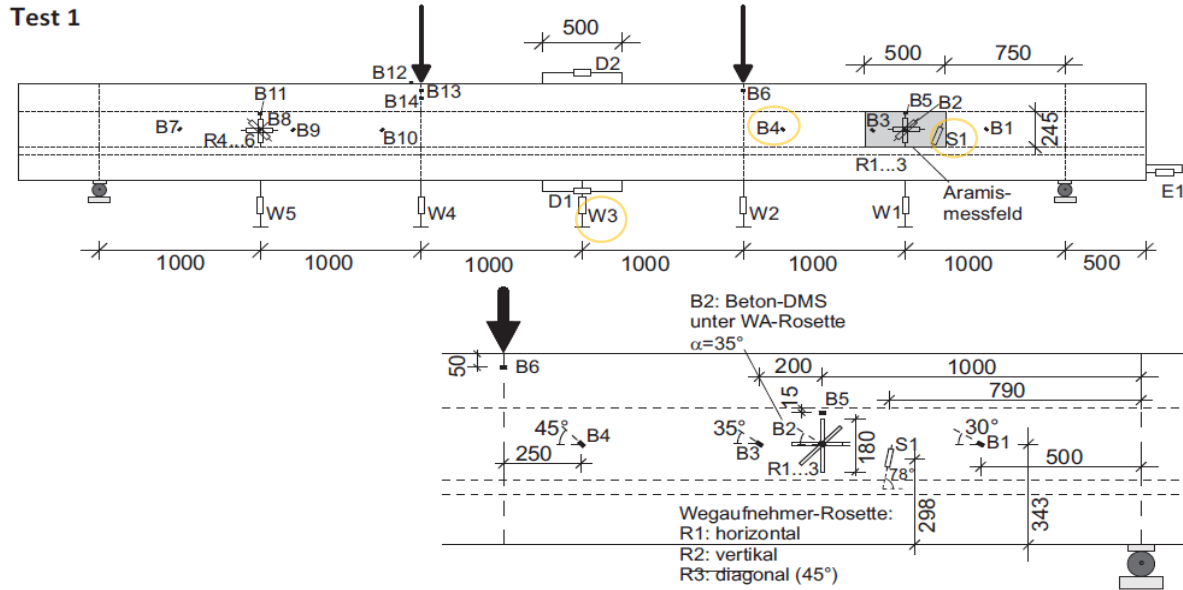


Figure 32: Metrology of concrete and sensors considered for comparison with the numerical results (Kurth 2012)

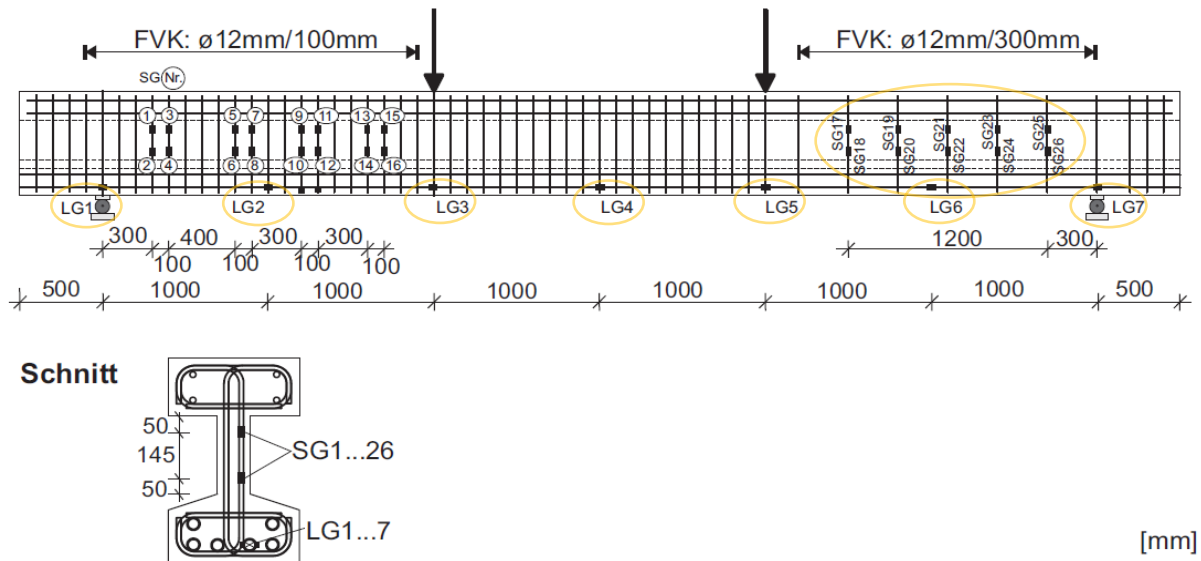


Figure 33: Metrology of reinforcement and sensors considered for comparison with the numerical results (Kurth 2012)

4.3.1.1 Load vs. displacement

In the Figure 34 the obtained deflection in the center of the beam through CONSHEAR and is presented and compared with the experimental results obtained by (Kurth 2012)

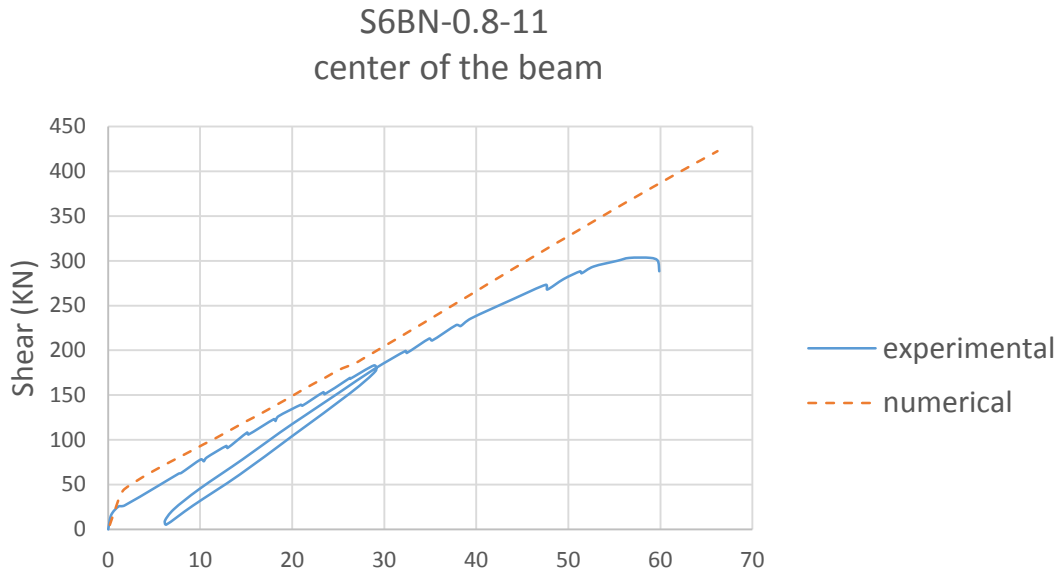


Figure 34: Experimental and numerical deflection in the center of the beam for test S6BN-0.8-11

As shown in Figure 34 the prediction of the model is similar to the experimental results.

However after cracking the results differ, this mismatch might be due to an overestimation of the concrete tensile strength (difficult to measure) and elasticity modulus.

After cracking the “tension stiffening” effect takes place which is the concrete contribution in the tension zone between the cracks. In the CONSHEAR model, tension-stiffening phenomenon is taken into account by the empirical equation of (Cervenka 1985)

The model is stiffer than the experimental test. The assumed smeared cracking approach ignores localized crack behaviour, such as slip between crack boundaries and bond-slip of the tension chord, which can also be a cause for this difference. Also, other factors related with the experimental tests such as deformation and pre-cracking of the beams due to shrinkage/creep or

other residual stress effects (that are not include in the numerical model) may contribute to this difference.

The model overestimated the ultimate load, predicting failure for a load level of about 420 kN, while the experimental is of 300 kN.

In relation to the deformation the model presents good fitting with the experimental results with a total displacement of about 65mm.

4.3.1.2 Strains in the FRP longitudinal reinforcement

Figure 35 presents the strains in the longitudinal reinforcement in 7 different sections along the beam , both experimental by (Kurth 2012) and those obtained numerically by the CONSHEAR model. The results shown correspond to different load levels.

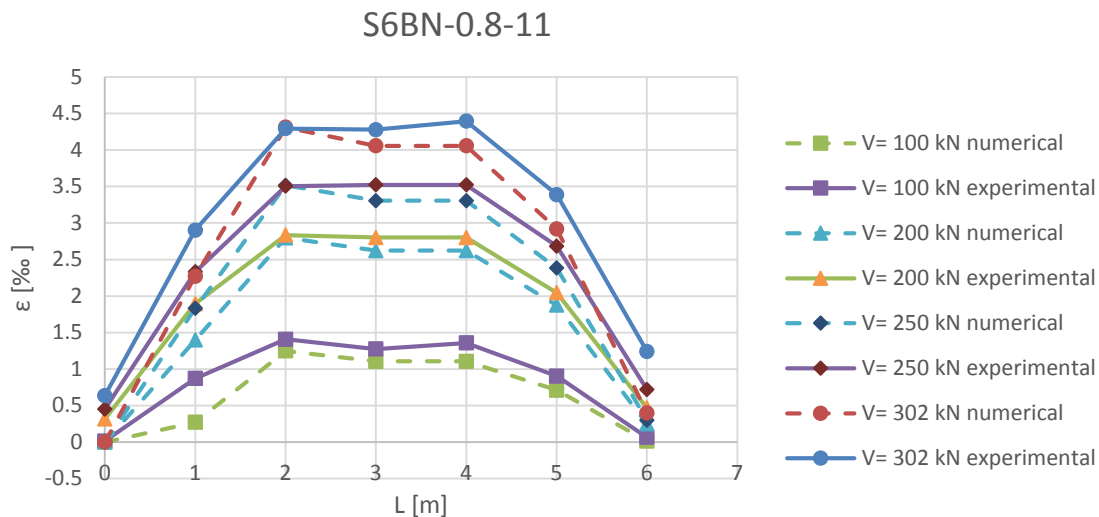


Figure 35: Experimental and numerical results for the strains in longitudinal FRP reinforcement for test S6BN-0.8-11

An overall correct fitting between numerical and experimental results is observed. It can be observed that the model prediction at smaller loads (V=100kN) is under the experimental strain

results, this is because the beam tested had a concrete tensile strength lower than the one considered in the model, although for higher loads the model fits better.

4.3.1.3 Strains in the FRP transversal reinforcement

Figure 36 represents the deformation of the stirrups that are situated in the right side of the beam; the location of the sensors are presented in the metrology of reinforcement in Figure 19.

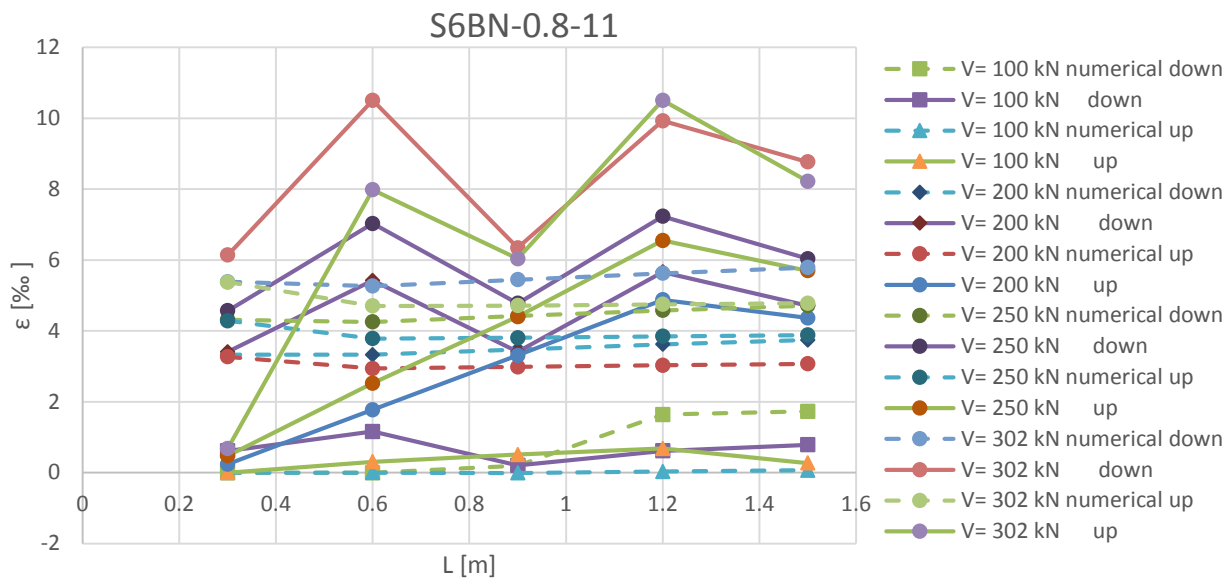


Figure 36 : Experimental and numerical results of Strains in stirrups along the length of the beam for test S6BN-0.8-11

Considering that this is a very local parameter that is being compared, and very influenced by the position of the cracks, a general acceptable fitting can be observed between the numerical and experimental results. The order of magnitude of the numerical results are in correspondence with average experimental measurements for each load level. The strain peaks observed in experimentation relate to crack interference (when a crack intersects the transversal reinforcement in the position of a sensor, it will cause a peak of deformation) and are not possible to be captured by a numerical model that is based on the smeared crack approach.

Other sources of damage in the experimental testing that can contribute to the difference are the possible damage due to shrinkage, creep and transportation. This would diminish the contribution of concrete resistance, thus making the load be absorbed more by the FRP stirrups.

4.3.1.4 Longitudinal strains in concrete

Figure 37 presents the concrete strains in the mid span of the beam for different load levels.

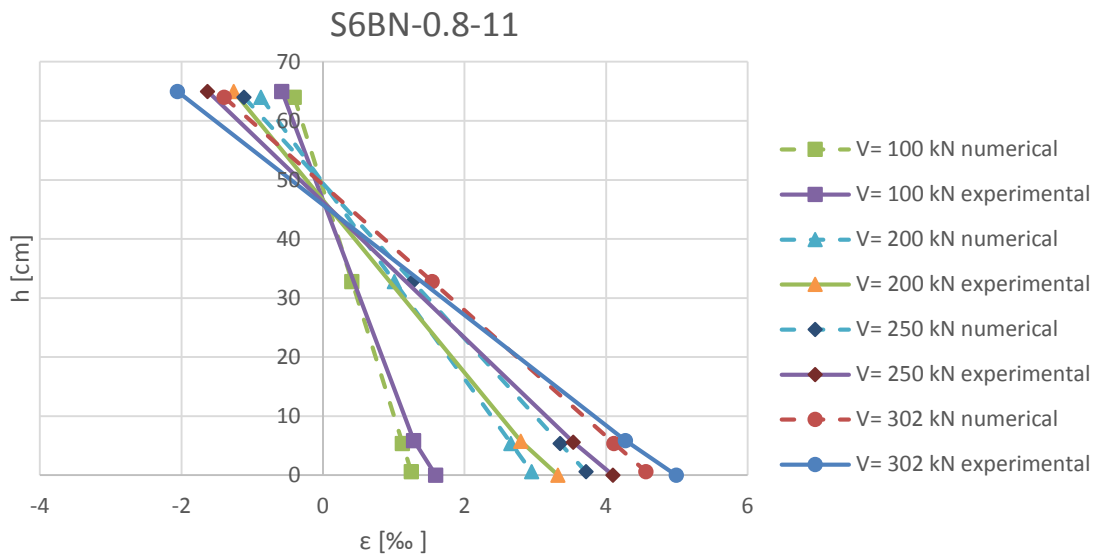


Figure 37: Experimental and numerical results of concrete deformation for test S6BN-0.8-11

As can be seen, the predicted results show a great similarity with the experimental ones. Only a small difference is seen in the load level ($V=100\text{kN}$). The experimental deformations are of 1.25% ($1.25 \cdot 10^{-3}$) in the bottom part (tension) for shear value $V=100\text{ kN}$, and our numerical results in the bottom part are 1.6% ($1.6 \cdot 10^{-3}$). This is, again, due to the possibility that the beam was pre-cracked, causing a decrease in tensile strength of the concrete. For higher load levels, the fitting is very good.

4.3.1.5 Transversal strain in the concrete web

Transversal strains in the concrete web measured by the strain rosette are compared with the numerical results in Figure 32.

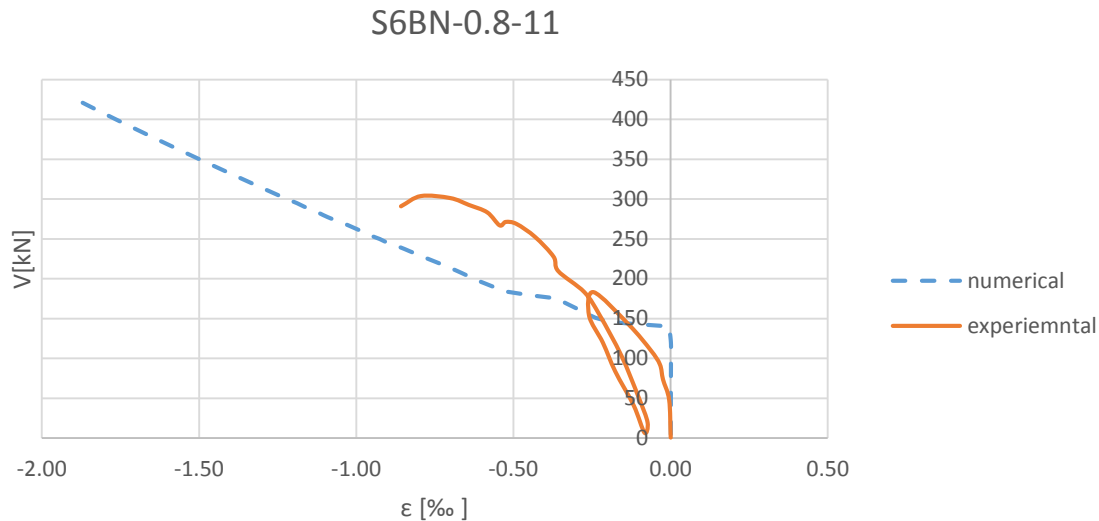


Figure 38: Shear-strain of concrete numerical and experimental results for test S6BN-0.8-11

The numerical approach overestimates the start of concrete cracking with about 100 kN. This is again due to our model being stiffer. Even though it can be observed that the model represents the experimental data, being capable of capturing the start of the diagonal cracking that corresponds to the load level for which the strains increase abruptly. Again, experimental measurements in this location (web of the beam) are very vulnerable to the effects of cracking.

4.3.1.6 Crack patterns

The crack development on the two beams was numerically predicted by the use of the discrete representation algorithm presented in chapter 3.1.5. Table 11 represents the development of cracking with increasing load predicted by the model and the comparison with the experimental observations for the ultimate load state. Numerical predictions, in terms of crack propagation and inclinations, show a fairly good agreement with the experimental evidence. It is interesting to

observe that the cracks develop more in the shear critical zone (right span of the beam). The beam reached an ultimate shear force $V=302\text{kN}$ and has a stirrup failure.

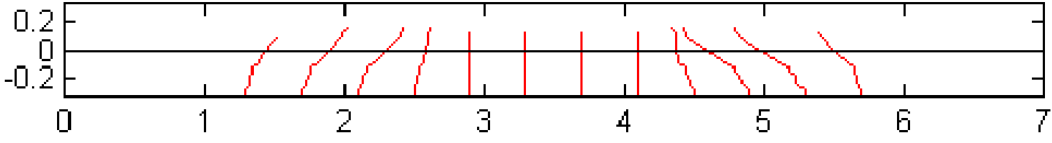
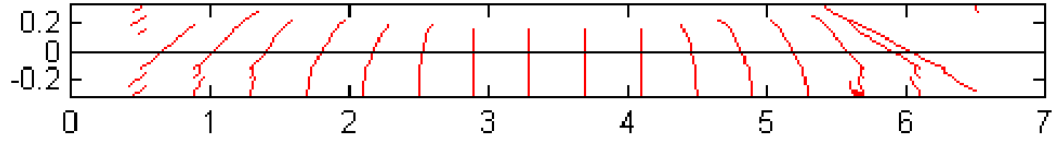
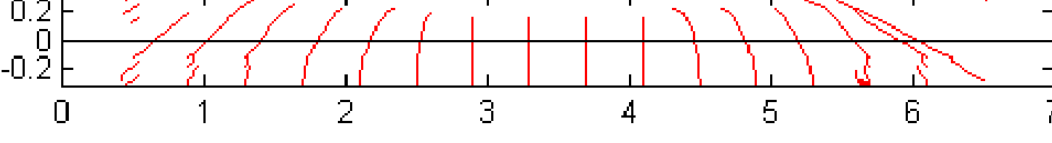
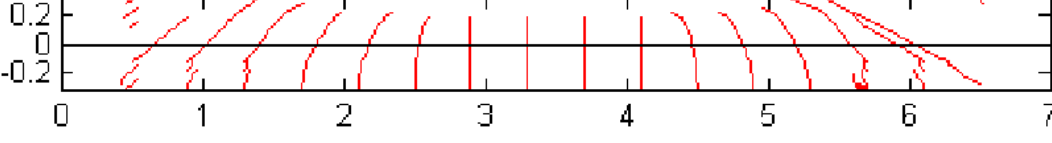

Cracking patterns	Shear force
 <p>A line graph showing cracking patterns for a shear force of 100 kN. The x-axis represents the length of the beam from 0 to 7, and the y-axis represents the vertical displacement from -0.2 to 0.2. Red lines indicate the locations and orientations of cracks, which are primarily vertical and concentrated in the right half of the beam (shear critical zone).</p>	V=100kN
 <p>A line graph showing cracking patterns for a shear force of 200 kN. The x-axis represents the length of the beam from 0 to 7, and the y-axis represents the vertical displacement from -0.2 to 0.2. Red lines indicate the locations and orientations of cracks, showing an increase in the number and length of diagonal cracks in the right half of the beam.</p>	V=200kN
 <p>A line graph showing cracking patterns for a shear force of 250 kN. The x-axis represents the length of the beam from 0 to 7, and the y-axis represents the vertical displacement from -0.2 to 0.2. Red lines indicate the locations and orientations of cracks, with further development of diagonal cracks in the right half of the beam.</p>	V=250kN
 <p>A line graph showing cracking patterns for a shear force of 302 kN. The x-axis represents the length of the beam from 0 to 7, and the y-axis represents the vertical displacement from -0.2 to 0.2. Red lines indicate the locations and orientations of cracks, showing extensive diagonal cracking and some horizontal cracking in the right half of the beam.</p>	V=302kN
 <p>A photograph of the physical beam specimen showing the actual cracking patterns. A black arrow points to the top surface of the beam, and a triangle symbol is located at the bottom right. The beam shows extensive diagonal cracking in the right half, consistent with the cracking pattern plots above.</p>	Experimental results

Table 11: Cracking patterns at different load levels for test S6BN-0.8-11

Figure 39 represents the crack width in the shear critical area with increase load (experimental and numerical results).

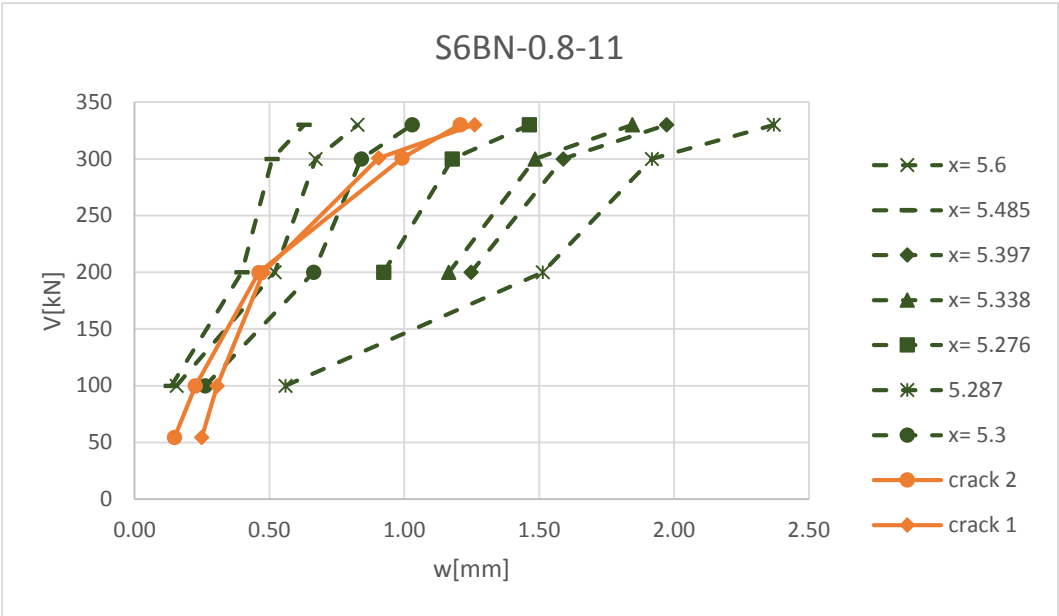


Figure 39: Cracking width for test S6BN-0.8-11

In relation to experimental results, Crack 1 and 2 represent the average crack width results measured experimentally with fiber optical sensors. The numerical results (as it is based on the smeared cracked approach and is not possible to monitor one single crack) correspond to average crack widths of different scanned areas; x distance measured in m from the left support of the beam until the left support (Figure 40)

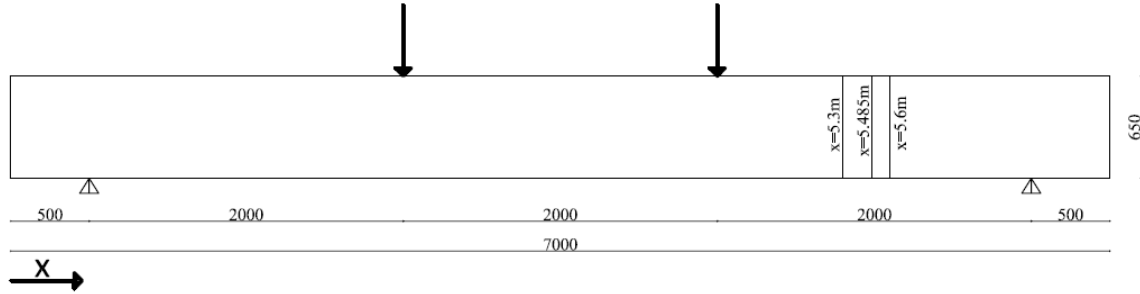


Figure 40: Location of measured cracks

Experimentally (Kurth 2012) obtained an average crack width of 1.2mm and a maximum crack width of 2mm which is similar with our numerical results that show a maximum crack width of 2.4mm at the ultimate shear force, and an average crack width of 1.5mm.

In the shear critical zone the biggest crack width forms.

It can be observed that the numerical results are consistent with the experimental observations, for all levels of damage.

It is difficult to compare the results because, in reality the discrete crack was measured with an optical sensor (ARAMIS), and the numerical results are obtained with a model based on the smeared crack approach that considers an average distribution of the crack in the element. Even though, the results present agree with the experimental ones in terms of order of magnitude and tendencies.

4.3.1.7 Other numerical results

Figure 41 presents the strains in transversal reinforcement for different heights in the cross section.

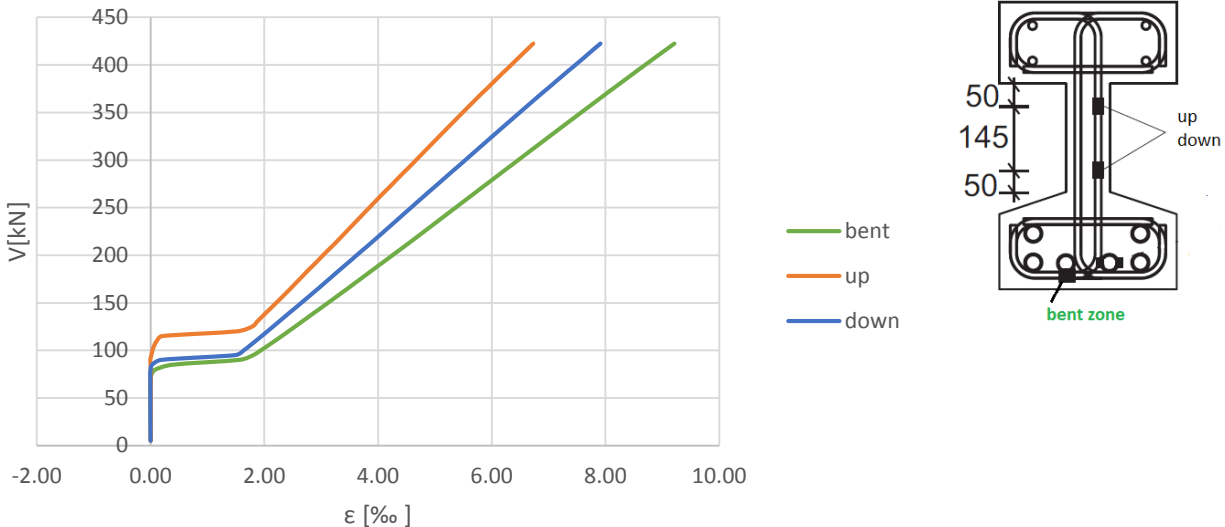


Figure 41: Strain in the stirrups for different positions of the sensors test S6BN-0.8-11

The up and down sensors corresponds to the ones described in (Kurth 2012)

Figure 33 (SG19 and SG20) which are situated at the middle of the stirrup, and the sensor in the bent zone is added by us to measure the strains in the failure zone of the stirrup.

As can be observed the strain in the bent zone is bigger 9.21‰ compared to 7.91 ‰ down, and 6.73‰ up, that is because the stirrups are more loaded when there is more damage, which is the bottom of the beam. When the cracking propagates to the top, the stirrups start to carry load.

Figure 42 represents the flow of strains in transversal reinforcement along the shear critical cross section for a load level of $V= 302 \text{ kN}$.

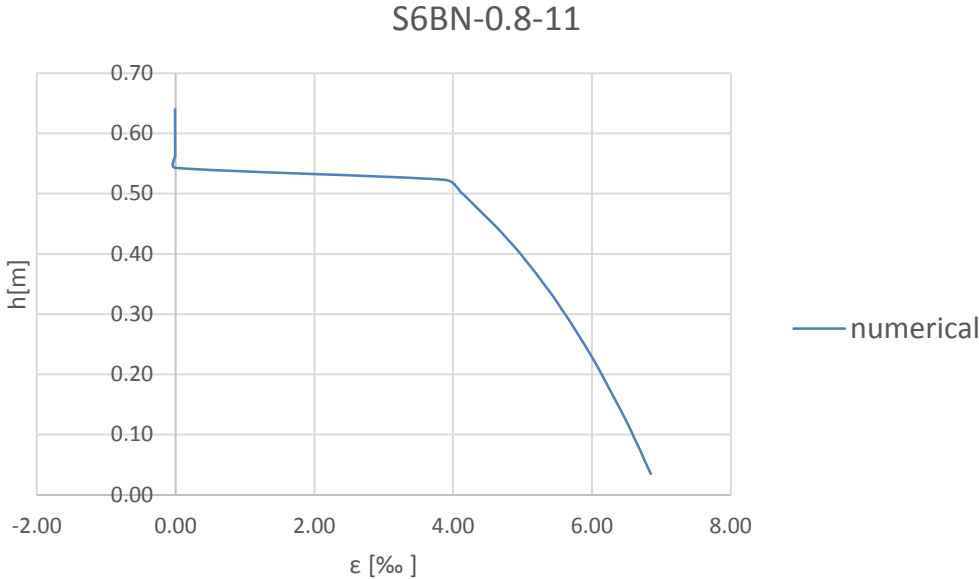


Figure 42: Strains in stirrup height at the bent zone for test S6BN-0.8-11

The same can be seen here. The bottom parts of the stirrups are more loaded than the top parts, and this is because we have more damage at the bottom and the top part in under compression, so the stirrups do not need to work.

4.3.2 Other tests beams

The results of the other test beams S2AN-0.8-3, S4AH-0.8-7, S8BH-0.8-15 and S10CN-0.7-19 are presented together in the following. This results present different tendencies and issues as the ones discussed in detail before; so no discussion is made specifically for these cases.

4.3.2.1 Load vs displacement

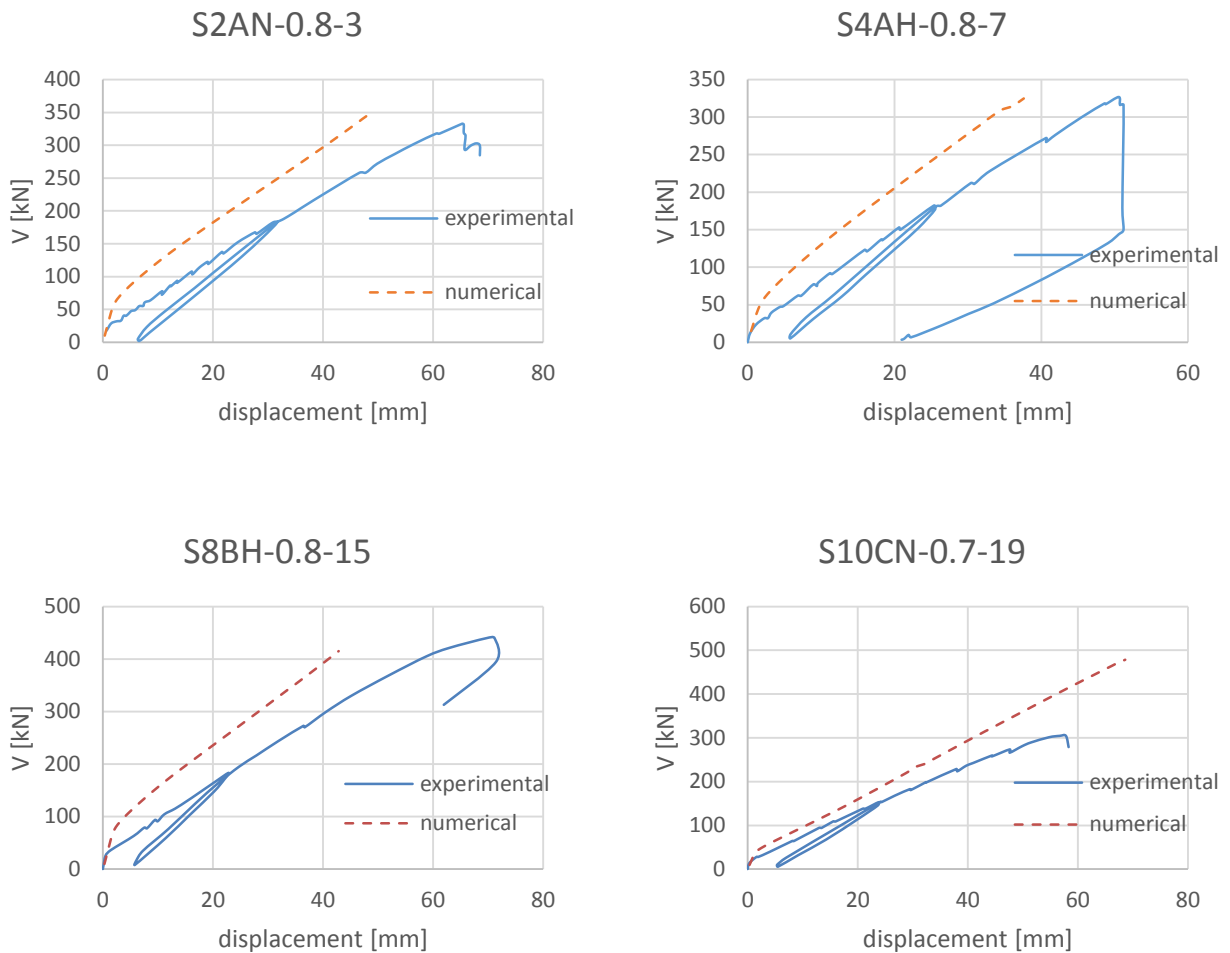


Figure 43: Experimental and numerical deflection in the center of the beam for tests S2AN-0.8-3, S4AH-0.8-7, S8BH-0.8-15 and S10CN-0.7-19

4.3.2.2 Strains in the FRP longitudinal reinforcement

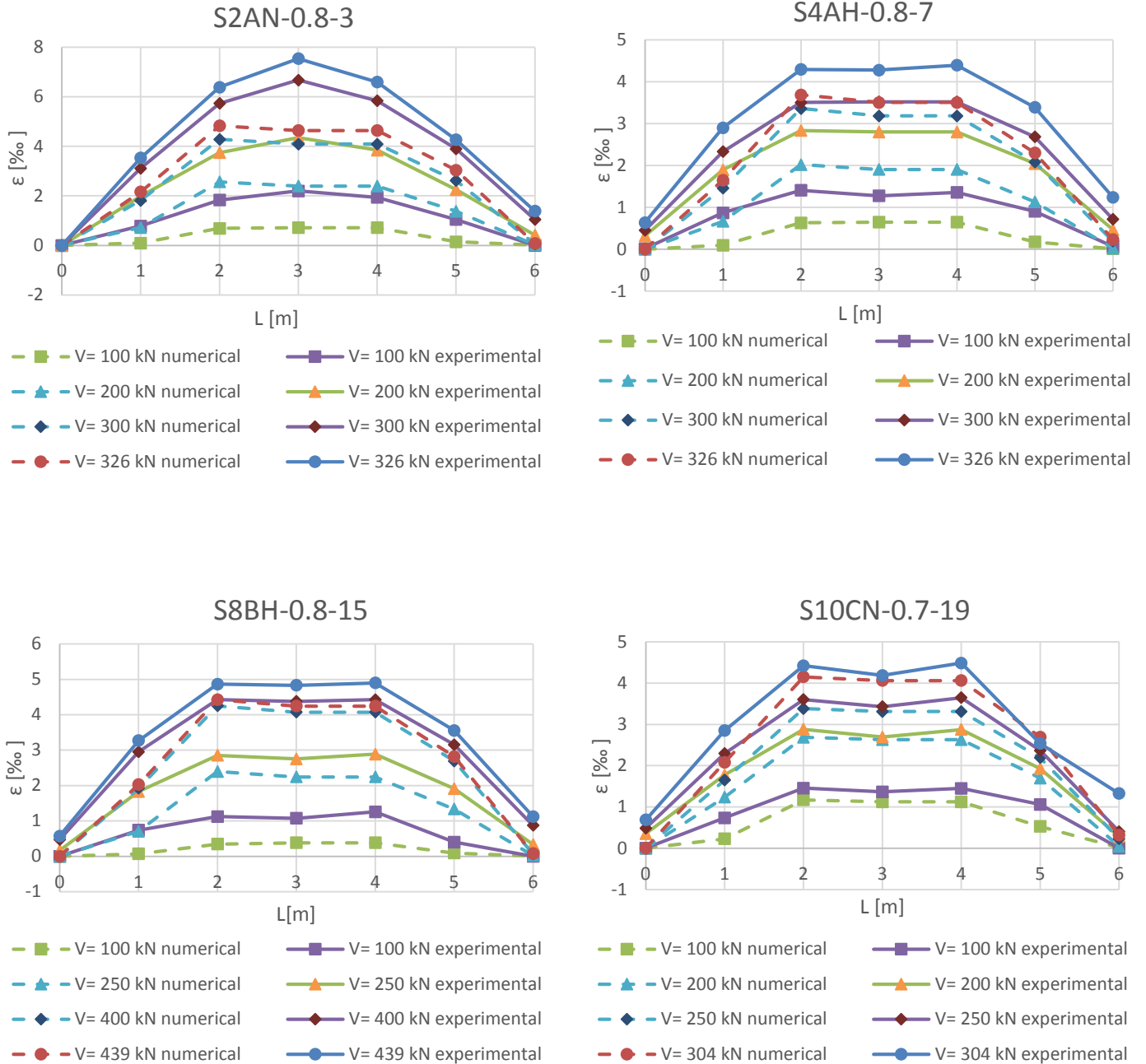
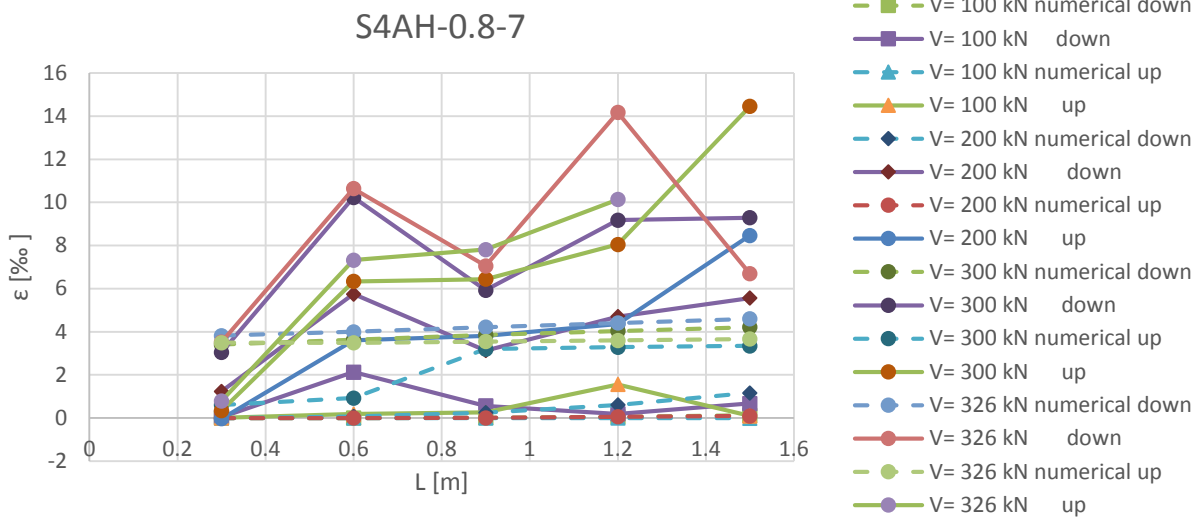
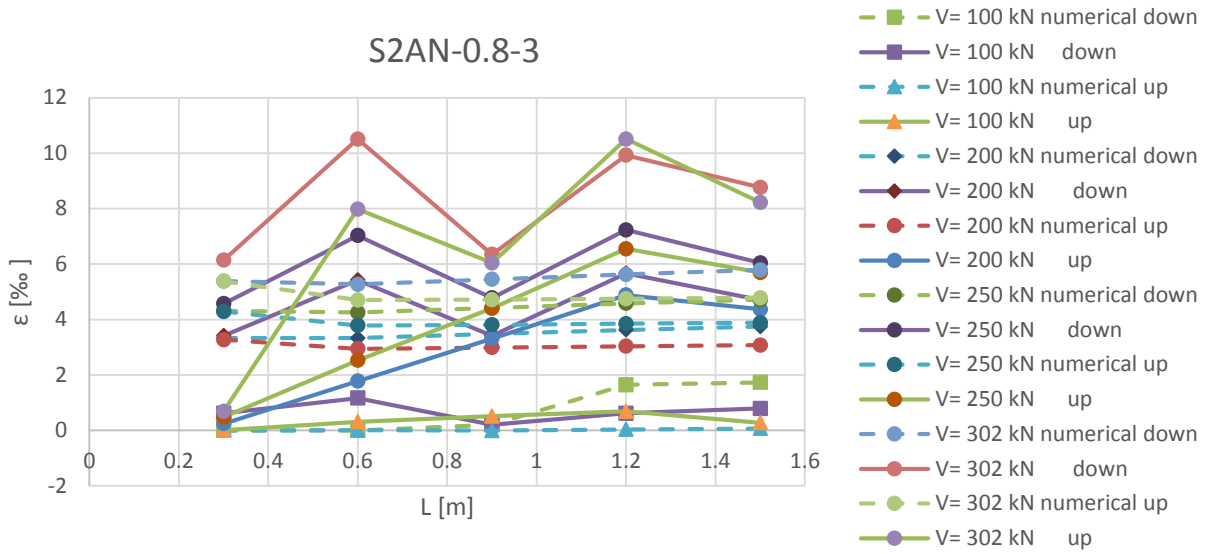


Figure 44: Experimental and numerical results of strains in the FRP longitudinal reinforcement for tests S2AN-0.8-3, S4AH-0.8-7, S8BH-0.8-15 and S10CN-0.7-19

4.3.2.3 Strains in the FRP transversal reinforcement



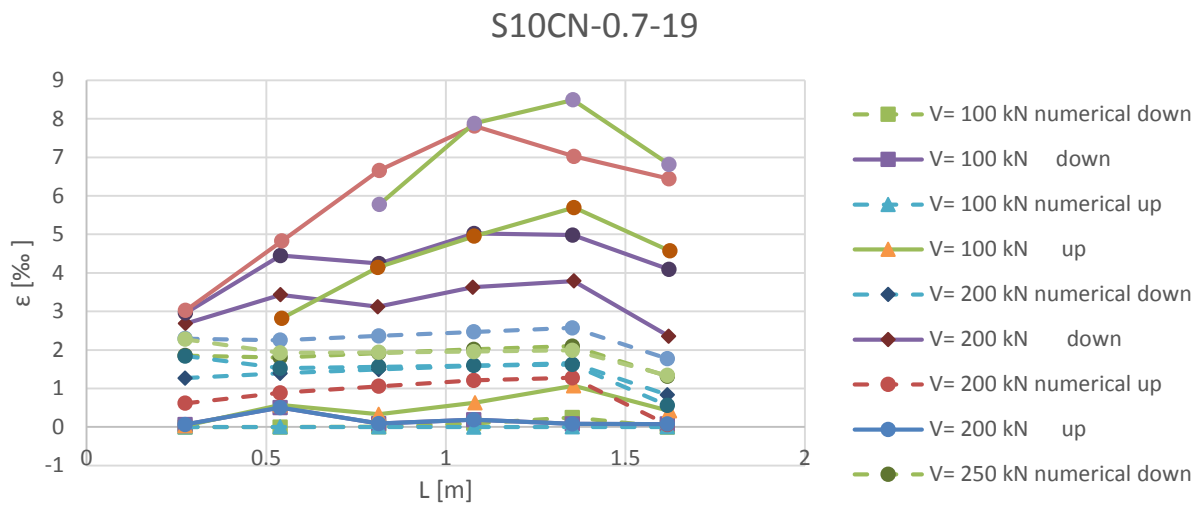
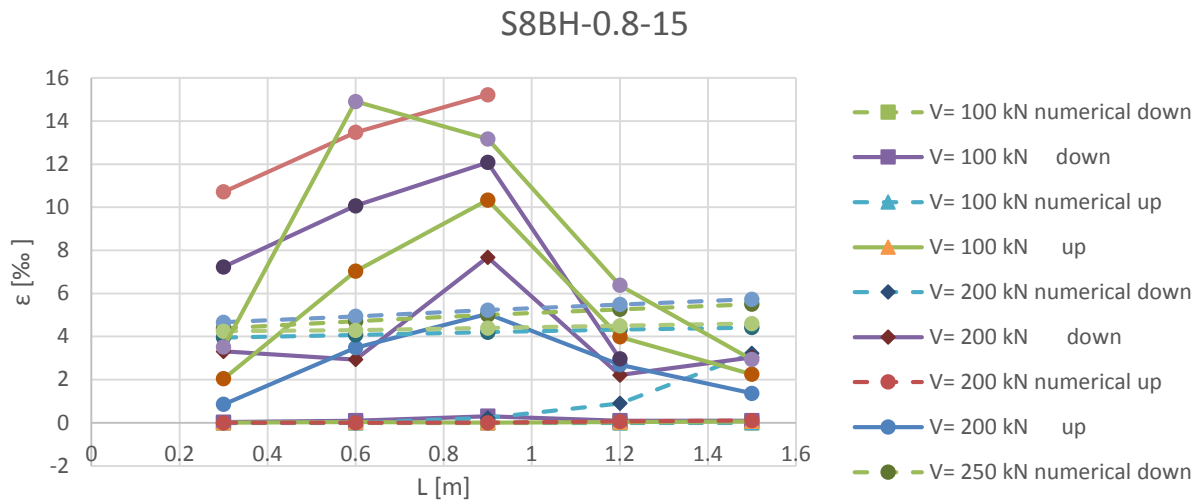


Figure 45: Experimental and numerical results of strains in stirrups along the length of the beam for tests S2AN-0.8-3, S4AH-0.8-7, S8BH-0.8-15 and S10CN-0.7-19

4.3.2.4 Longitudinal strains in concrete

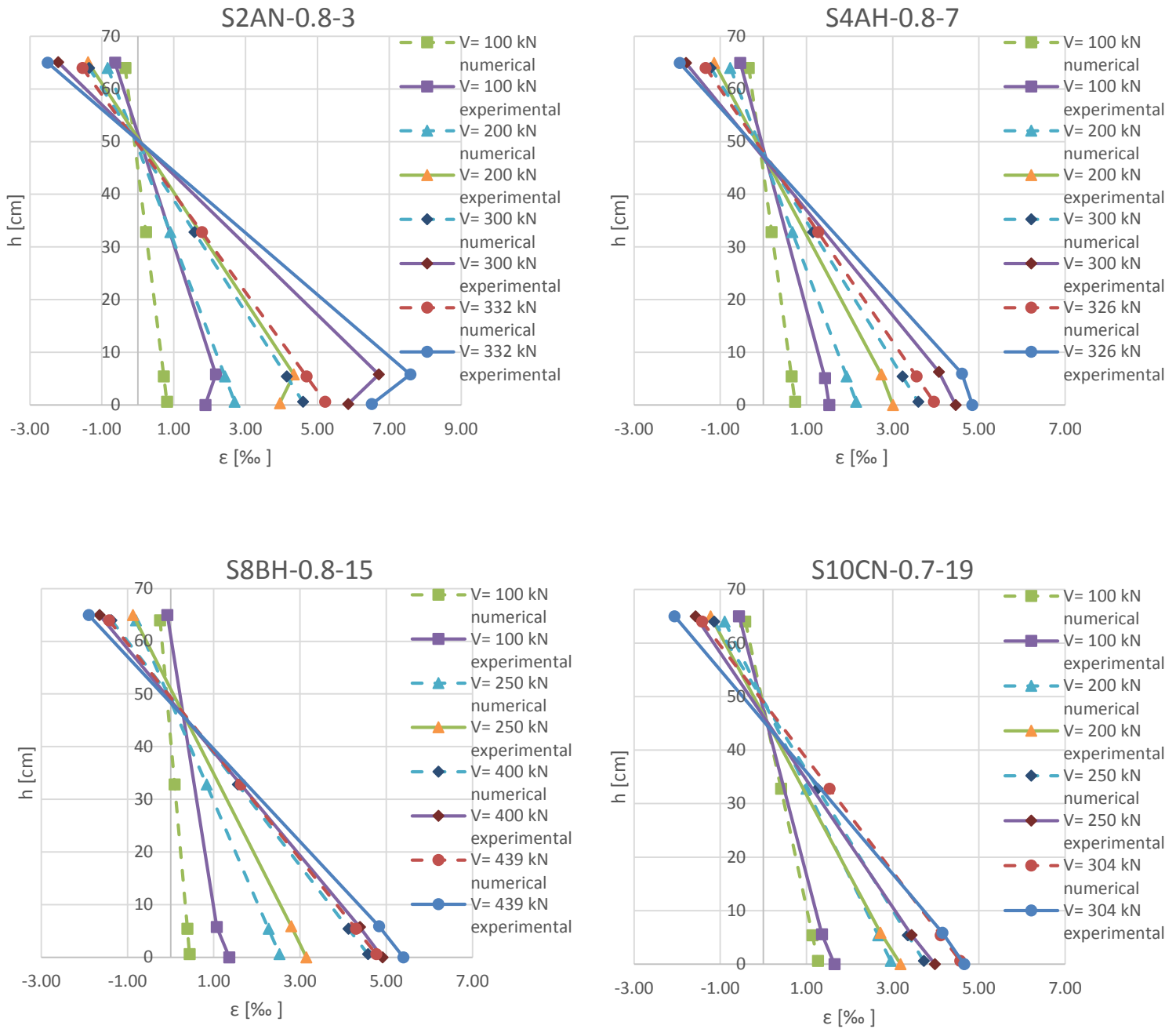


Figure 46: Experimental and numerical results of longitudinal concrete deformation for tests S2AN-0.8-3, S4AH-0.8-7, S8BH-0.8-15 and S10CN-0.7-19

4.3.2.5 Transversal strain in the concrete web

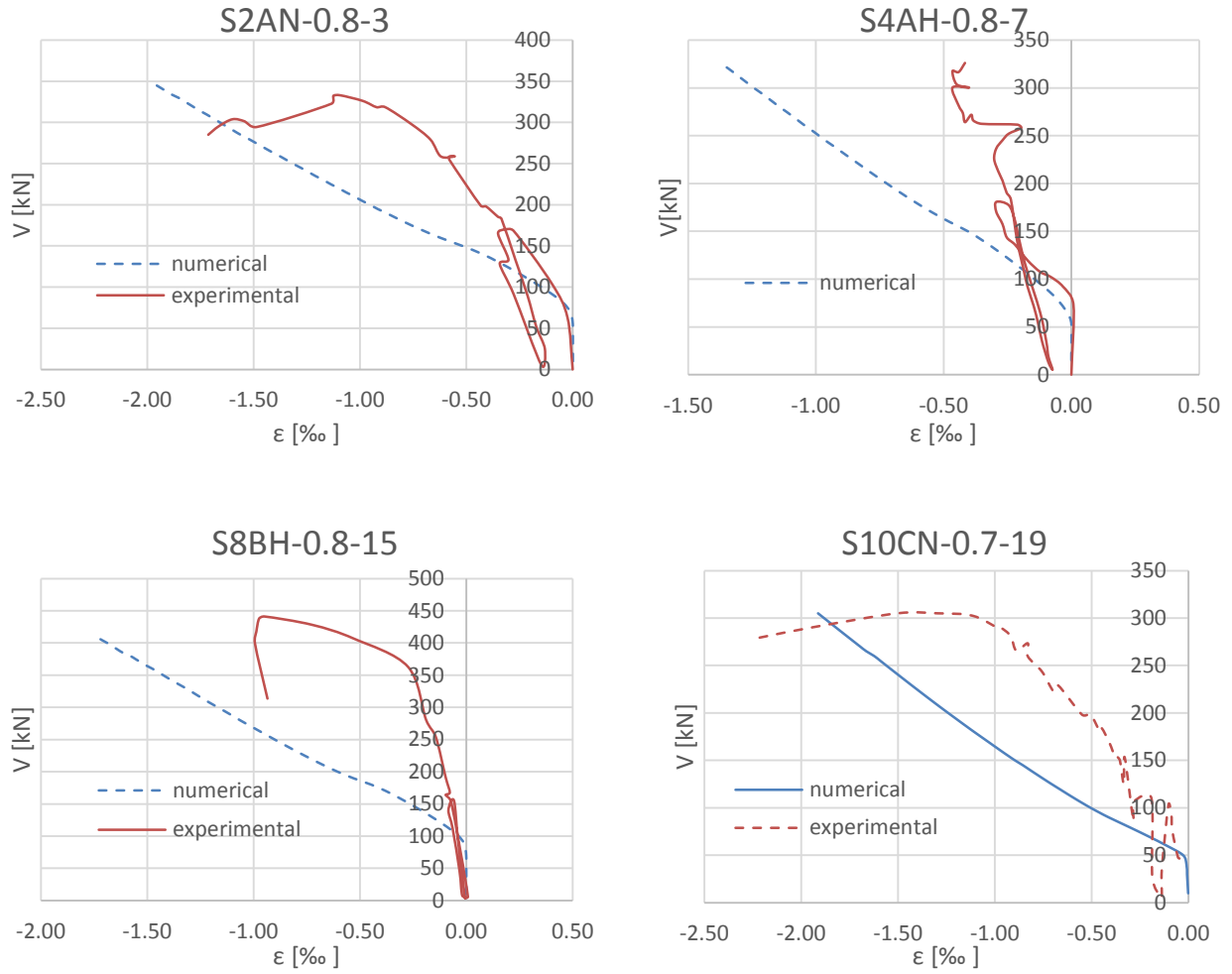


Figure 47: Numerical and experimental of transversal strain in the concrete web results for tests S2AN-0.8-3, S4AH-0.8-7, S8BH-0.8-15 and S10CN-0.7-19

5 Conclusions

This work was motivated by the increasing popularity of FRP composites in the field of structural engineering. The advantages offered by the FRP as passive reinforcement lies largely in its resistance to corrosion, high strength and stiffness and low weight when compared to steel.

However the application of this material in construction is still limited by the lack of experimental and numerical investigations that can support reliable codes of practice. This is especially problematic in the shear mechanisms, as this problem is not even yet solved for traditionally reinforced concrete structures with steel.

Experimental works allied to numerical simulations can contribute to a better understanding of this specific structural problem.

This thesis provides a discussion of the state of the art on the problematic of FRP reinforcement and the resistance of shear. An experimental campaign available in literature, with concrete specimens with longitudinal and transversal reinforcement, tested in shear, was simulated numerically by means of FE model.

Concerning the overall experimental results reported in the literature, FRP RC beams present different shear failure modes when compared with the traditional RC beams: either present failure due to rupture of the FRP stirrups in the bent zone or fail due to concrete crushing of the struts between inclined shear cracks or due to crushing at the concrete chord. These failure mechanisms observed in the experiments should be considered in the formulation of the theoretical models to evaluate the shear strength of FRP RC beams with FRP stirrups. In this sense, numerical models can bring an important contribution.

In this thesis, the numerical results obtained through the use of 1D fiber model, CONSHEAR, were compared to the experimental ones conducted by (Kurth 2012) in terms of ultimate load, displacements, strains in the concrete, longitudinal and transversal FRP reinforcement and diagonal cracking pattern

The following conclusions can be drawn from the studies performed:

1. The 1D model reproduces with reasonable accuracy the ultimate load, the load–deflection behaviour, the longitudinal and transversal strains in the concrete, the strains in the longitudinal FRP reinforcement with increasing load.
2. Regarding the strains in the transversal FRP reinforcement a general acceptable fitting resulted, considering that the strain peaks are not possible to be captured by a numerical model that is based on the smeared crack approach.
3. As observed the numerical results of shear deflections at mid-span present higher estimations of shear displacement, this might be due to an overestimation of the concrete tensile strength that is difficult to measure and elasticity modulus. Another cause for this overestimation is the fact that the program is based on the smeared crack approach which ignores localized crack behaviour such as slip between crack boundaries and bond-slip of the tension chord.
4. The cracking behaviour was obtained in terms of crack width and cracking patterns for different load levels. The model slightly overestimates the maximum and the average crack widths. The model is capable to obtain the development of damage with increasing load in terms of number, inclination and height of cracks.
5. Regarding the failure modes in the experiments with high shear reinforcement ratios, from $\rho_w = 2.22\%$ to $\rho_w = 2.26\%$, failure occurred by crushing of concrete in the web. The specimens with lower shear reinforcement ratios ($\rho_w = 0.45$ and 0.75%) and presented failure of the transversal reinforcement, due to a combined shear-tensile stress locally present in the region of the main shear crack, and the specimens with medium shear reinforcement ratios ($\rho_w=1.26\%$) presented both types of failure.
6. The failure of the tested FRP stirrups always occurred at the bent zone due to the bending of the FRP bars into the stirrups configuration, significantly reduces its strength at the bent portions, due to their unidirectional characteristics.

7. In case that a local rupture of the stirrups at the bent zone does not occur, and due to the high strength of the FRP rebars, a concrete crushing failure at the compression chord can develop at the load application point
8. The strain in the bent zone is bigger 9.21‰ compared to 7.91 ‰ down, and 6.73‰ up, that is because the stirrups are more loaded when there is more damage, which is the bottom of the beam. When the cracking propagates to the top, the stirrups start to carry load.
9. Regarding the strains in the longitudinal reinforcement, a good fit is obtained for lower and high load levels. It should be noted that a good correspondence between the experimental and numerical results is only possible to work with models that take into account the shear, so that the increase in deformation of the longitudinal reinforcement because of the shear effect is considered.
10. Referring to the strains in the concrete the numerical model is capable of capturing the start of the diagonal cracking that corresponds to the load level for which the strains increase abruptly, though slightly overestimates the starting crack force.

This work opened the following future lines of work:

- Validate the numerical model more deeply by simulating more tests from the experimental database of (Kurth 2012) and others
- Compare the second test of this experimental campaign using a phased analysis to capture the damage produced by the first set of tests.
- Analyze the influence of the effective flange width in the shear resistance predicted by the numerical model by comparing several numerical analysis with different areas of the compressed flange contributing to the shear resistance.
- Compare the maximum strains in FRP in the bent zone with the limits imposed by actual codes and proposals and discuss if these are over-conservative and contribute to a more efficient determination of this limitation.
- Use the validated numerical model to develop new analytical equations for design.

References

- ACI-440.1R-06, 2006. Guide for the Design and Construction of Structural Concrete Reinforced with FRP Bars. , p.44.
- Ahmed, E. a., El-Salakawy, E.F. & Benmokrane, B., 2010. Shear Performance of RC Bridge Girders Reinforced with Carbon FRP Stirrups. *Journal of Bridge Engineering*, 15(1), pp.44–54.
- Alzate, A., 2012. Análisis de los modelos de comportamiento de vigas de hormigón armado reforzadas a cortante con polímeros armados con fibras (FRP). Validación y calibración experimental. *Tesis doctoral, UPM, Departamento de mecánica de los medios continuos y teoría de estructuras, Instituto Eduardo Torroja de Ciencias de la Construcción*.
- BaNthia, N. et al., 2006. ISIS Educational Module 2: An Introduction to FRP Composites for Construction. *ISIS Canada Educational Module*.
- Bentz, E.C., Massam, L. & Collins, M.P., 2010. Shear Strength of Large Concrete Members with FRP Reinforcement. *Journal of Composites for Construction*, 14(6), pp.637–646.
- Cervenka, V., 1985. Constitutive model for cracked reinforced concrete. *ACI Journal Proceedings*, 82(82), pp.877–882.
- Clarke, J.L., 1996. FRP reinforced concrete structures. *2nd International Conference on Advanced Composite Materials in Bridges and Structures, Montreal, Quebec, Canada*, pp.41–48.
- CNR-DT 204/2006, Guide for the Design and Construction of Fiber-Reinforced Concrete Structures. *2006.Rome,Italy*.
- CSA S806-12, C. S. Association. Design and construction of building components with fibre reinforced polymers. *Toronto, Canada. 2012*.
- El-Ghandour et al., 1999. New Approach for the Punching Shear Capacity Prediction of FRP RC Flat Slab. *Fourth International Symposium Fiber Reinforced Polymers for Reinforced Concrete Structures (FRPRCS- 4)*, (Baltimore (USA)), pp.135–144.
- El-Ghandour, A. W., Pilakoutas, K. & Waldron, P., 1998. Use of FRP Reinforcement for Concrete Plate Elements. *International Conference on Advanced Composites, ICAC 98,, (Hurghada, Egypt)*, pp.353–361.
- El-Sayed, A.K. & Soudki, K., 2011. Evaluation of Shear Design Equations of Concrete Beams with FRP Reinforcement. *Journal of Composites for Construction*, 15(1), pp.9–20.

- Ferreira, D. et al., 2013. Nonlinear analysis of RC beams using a hybrid shear-flexural fibre beam model. *Engineering Computations*, 31(7), pp.1444–1483.
- Ferreira, D.C.S., 2013. Computer Program CONSHEAR Nonlinear analysis of concrete structures critical to shear. , (April).
- Fico, R., Prota, A. & Manfredi, G., 2008. Assessment of Eurocode-like design equations for the shear capacity of FRP RC members. *Composites Part B: Engineering*, 39(5), pp.792–806.
- Hegger, J., Kurth, M. & Niewels, J., 2009. Shear Analysis of Concrete Members With Fiber-Reinforced Polymers (Frp) As Internal Reinforcement. *Concrete*, (July), pp.13–16.
- JSCE, 1997. Recommendations for design and construction of concrete structures using continuous fiber reinforcing materials. *Japan Society of Civil Engineers.*, C, p.325.
- Kurth, M., 2012. Kurth RWTH Disse Querkrafttragverhalten Faserverbundkunststoffe 2012-12.
- Mari, A.R., 2000. Numerical simulation of the segmental construction of three dimensional concrete frames. *Engineering Structures*, 22(6), pp.585–596.
- Nagasaka, T., Fukuyama, H. & Tanigaki, M., 1933. Shear performance of concrete beams reinforced with FRP stirrups. 1993. Detroit, Michigan.
- Nehdi, M., El Chabib, H. & Saïd, a. A., 2007. Proposed Shear Design Equations for FRP-Reinforced Concrete Beams Based on Genetic Algorithms Approach. *Journal of Materials in Civil Engineering*, 19(12), pp.1033–1042.
- Niewels, J., 2008. Zum Tragverhalten von Betonbauteilen mit Faserverbundkunststoff-Bewehrung. *Thesis*.
- Pilakoutas, K., 2000. Failure Analysis of Industrial Composite Materials, E. E. Gdoutos, K. Pilakoutas, and C. A. Rodopoulos, eds., McGraw-Hill, *Composites in Concrete Construction*, (London), pp.449–497.
- Shehata, E., Morphy, R. & Rizkalla, S., 2000. Fibre reinforced polymer shear reinforcement for concrete members: behaviour and design guidelines. *Canadian Journal of Civil Engineering*, 27(5), pp.859–872.
- Spadea, S., 2010. Comportamento di elementi di calcestruzzo armato con barre di materiale composito fibroinforzato. *University of Salerno, Fisciano, Italy*.
- Zararis, I.P., Karaveziroglou, M.K. & Zararis, P.D., 2006. Shear strength of reinforced concrete T-beams. *ACI Structural Journal*, 103(5), pp.693–700.

Zhao, W., Maruyama, K. & Suzuki, H., 1995. Shear behaviour of concrete beams reinforced with FRP rods as longitudinal and shear reinforcement. In: Proceedings of the 2nd international RILEM symposium non-metallic (FRP) reinforcement for concrete structures (FRPRCS-2); 1995. p. 352e9.